A Study on a Log-linearized Peripheral Arterial Viscoelastic Model for Medical Applications

（医療応用を目的とした対数線形化末梢血管粘弾性モデルに関する研究）

by

Hiroki HIRANO

Graduate School of Engineering
Hiroshima University

March, 2016

Contents

List of Figures

List of Tables

Chapter 1

Introduction

1.1 Background

The autonomic nervous system incorporates involuntary control functions for circulation, respiration, digestion, body temperature, incretion, reproduction and metabolism. It has sympathetic and parasympathetic parts, which have opposite actions. The former is activated by physical activity such as exercise or by stress caused by stimuli such as fear, anxiety, bleeding or pain, which increase the heartbeat and vascular contraction [1]. The latter is activated by relaxing activities such as sleep or eating, which reduce the heartbeat and vascular dilatation [1]. In this way, there is a close relationship between autonomic nerve activity and biological response.

The many medical conditions caused by autonomic nervous function abnormalities include hyperhidrosis, which is characterized by excessive sweating unrelated to body temperature and stems from sympathetic nerve hyperactivity. It affects areas with a high concentration of sweat glands such as the hands, lower limbs and armpits. Palmar and footpad hyperhidrosis in particular cause misery for sufferers. Japan's Ministry of Health, Labour and Welfare reports that the total number of people with serious hyperhidrosis is as high as 0.8 million [2]. The first stage of hyperhidrosis treatment involves dermatological approaches such as external application of aluminum chloride and

electrical therapy on the skin surface [3]. For severely affected patients who remain unresponsive to such treatment, a surgical operation known as endoscopic thoracic sympathectomy (ETS) is performed [3]. In this procedure, a clip is used to block the sympathetic trunk, whose excessive activity causes hyperhidrosis, near the spine of the thorax [4]. If this is insufficiently effective the first time, it is performed again. To support accurate assessment for the success or failure of ETS, the ability to monitor sympathetic nerve activity beyond the distal area of the blocked part is essential.

Meanwhile, numerous disorders appear to have the characteristics of autonomic nervous system conditions but in fact are not. An example of this is Parkinson's disease, which is a generic name for a condition involving the pathognomonic motor symptoms of essential tremors, muscle rigidity, akinesia and impairment of postural reflexes [5]. Although the mechanism behind Parkinson's disease has not been fully elucidated, its motor symptoms are considered to stem from a reduced number of neurons in the substantia nigra and lower production of dopamine neurotransmitters [5]. Parkinsonism is a generic term describing a condition with several symptoms similar to those of Parkinson's disease [5]. The causes of Parkinsonism symptoms are obvious. For instance, drug-induced Parkinsonism occurs as a result of side effects from tranquilizers or antipsychotic drugs, vascular Parkinsonism results from vascular conditions of the brain such as cerebral infarction and cerebral hemorrhage, and multiple-system atrophy is caused by cerebellar degeneration [5]. It is very important to discriminate between Parkinson's disease and Parkinsonism, as their treatment methods differ [5]. Doctors clinically diagnose Parkinson's disease and Parkinsonism based on information obtained by examining and asking patients questions using the Hoehn and Yahr scale [6] and the unified Parkinson's disease rating scale (UPDRS) [7]. However, it is challenging even for experienced doctors to distinguish the two conditions because their

motion impairment characteristics are similar. The Hoehn and Yahr scale and UPDRS also involve only subjective assessment by doctors and self-reporting by patients on motility issues [5]. To support diagnosis, Okuno *et al.* proposed a finger-tapping movement measurement system involving the use of an acceleration sensor [8], and Shima *et al.* proposed a similar system involving the use of a magnetic sensor [9]. Shima *et al.* also proposed a quantitative evaluation method based on UPDRS for Parkinson's disease. These methods incorporate the evaluation of finger-tapping function, and cannot be used to distinguish Parkinson's disease from Parkinsonism because they do not support evaluation of Parkinson's disease characteristics other than certain motor functions. However, Parkinson's disease sufferers exhibit symptoms discordant from those of Parkinsonism, including autonomic nervous symptoms such as reduced sweating, orthostatic hypotension, coprostasis and dysuria [5]. Monitoring of autonomic nervous function is therefore useful for differential diagnosis between the two conditions.

Monitoring of autonomic nerve activity is also useful for other diagnosis tasks such as evaluation of pain during surgery and treatment under anesthesia, which is given to inhibit pain and mental suffering during surgical operations. General anesthesia involves injecting the patient with a combination of an analgesic, a tranquilizer and muscle relaxant. These must be administered in appropriate amounts and with appropriate timing in consideration of individual conditions because excessive administration places a burden on patients [10,11]. The bispectral index (BIS) has been used to quantitatively and objectively estimate arousal levels based on brain waves in order to monitor sedation [12], and neuromuscular monitors have been used to quantitatively and objectively assess muscular contraction levels based on electrical stimuli in order to monitor muscle relaxation [13]. However, the analgesic effect is only subjectively estimated by doctors based on heart rate and brain wave changes; quantitative and

objective assessment of the pain actually felt by patients remains challenging. As the autonomic nervous system is activated by painful stimuli [1], the capacity for quantitative and objective determination of autonomic nerve activity would be useful for assessing pain levels in order to determine appropriate anesthesia dosages.

1.2 Related Works

Various methods for quantitative evaluation of autonomic nerve activity based on biological responses have been reported in previous literature [14–16, 18, 19, 21, 23, 27]. For example, Shahani *et al.* evaluated autonomic nerve activity based on sweat gland activity estimated from changes in the electrical potential of the skin surface [14]. However, electrical potential cannot be measured from patients with abnormal sweat gland function or skin abnormalities, and is profoundly affected by measurement conditions such as electrode positioning, room temperature and body temperature. Some researchers have proposed autonomic nervous function evaluation methods focused on arterioles and other parts of the circulatory system. By way of example, Akselrod *et al.*'s frequency analysis of intervals between canine heartbeats suggested that parasympathetic nerve activity is linked to the high-frequency component of these intervals (HF: 0.15 – 0.4 Hz), and that sympathetic nerve activity corresponds to their low-frequency component (LF: 0.15 – 0.4 Hz) per HF (i.e., LF/HF). This method, which is called heart rate variability (HRV) analysis, is applied in a variety of situations [15]. By way of example, surgical results of endoscopic thoracic sympathectomy (ETS) can be evaluated on the basis of changes in sympathetic nerve activity calculated from HRV before and after operations [16]; autonomic nervous function for patients with Parkinson's disease calculated from HRV can be non-invasively evaluated via head-up tilt tests [17] in which the subject stands passively [18]; and pain/discomfort experienced

by patients during dental treatment can be estimated from HRV [19]. However, HRV supports comprehensive assessment only for effects relating to the autonomic nervous system due to its focus on cardiac autonomic nerve activity [20]. When peripheral autonomic nerve activity needs to be quantitatively evaluated (as is the case with ETS), HRV analysis is unsuitable because it does not support elucidation of changes in local autonomic nerve activity in response to stimuli during online surgical operations and treatment. Patients with Parkinson's disease or Parkinsonism are also often elderly and may have arrhythmia, which precludes the application of HRV analysis due to the associated limitations such as arrhythmias. It is also difficult to evaluate acute pain during surgery and treatment because HRV analysis results cannot be provided immediately due to the delay associated with the window determined by the low-frequency band (i.e., 0.04 – 0.4 Hz) used to evaluate autonomic nerve activity.

Meanwhile, it is well known that peripheral arteries including in arterioles are regulated by the sympathetic nervous system, and acutely show responses such as contraction and relaxation of arteries associated with disturbance [20]. To support the evaluation of autonomic nerve activity with focus on changes in peripheral arterial condition, Korhonen *et al.* reported that photoplethysmogram (PPG) amplitude is reduced when the subject experiences pain [21]. However, Nakamura *et al.* reported that this amplitude may be unsuitable for the evaluation of autonomic nerve activity when blood pressure changes in the absence of autonomic nerve activation because photoplethysmograms are affected by such change [22]. Sakane *et al.* proposed a method for estimating the dynamic characteristics of peripheral arterial walls, which depend on linear stiffness, viscosity, inertia and other aspects of mechanical impedance [23]. Figure 1.1 shows an overview of the peripheral arterial dynamics characteristics proposed by Sakane *et al* [23]. To support the monitoring of sympathetic nerve activity

during ETS, Sakane *et al.* expressed the impedance characteristics of arterioles and other parts of the peripheral vascular system as well as arteries from the fingertip to the wrist with photoplethysmograms and radial arterial pressure:

$$dP_b(t) = \tilde{M}d\ddot{P}_l(t) + \tilde{B}d\dot{P}_l(t) + \tilde{K}dP_l(t). \tag{1.1}$$

Here, $dP_b(t) = P_b(t) - P_b(t_0)$, $dP_l(t) = P_l(t) - P_l(t_0)$, $d\dot{P}_l(t) = \dot{P}_l(t) - \dot{P}_l(t_0)$, $d\ddot{P}_l(t) = \ddot{P}_l(t) - \ddot{P}_l(t_0)$; $P_b(t)$, $P_l(t)$, $\dot{P}_l(t)$ and $\ddot{P}_l(t)$ are arterial pressure, the photoplethysmogram, the photoplethysmogram rate, and photoplethysmogram acceleration, respectively. t_0 is the time relative to the phase (e.g., R-wave timing) at any time in the cardiac cycle. $\tilde{M}$, $\tilde{B}$ and $\tilde{K}$ represent the inertia, viscosity and stiffness of the arterial wall, respectively. Sakane *et al.* showed that the stiffness parameter $\tilde{K}$ reflects changes in sympathetic nerve activity during ETS, and proposed the stiffness parameter $\tilde{K}$ as an index for monitoring sympathetic nerve activity during ETS. The relationship between blood pressure and arterial diameter in the aorta of Sakane's model is assumed to be linear. However, other researchers have experimentally established that this relationship has a nonlinear characteristic [24–26]. As a result, the stiffness parameter $\tilde{K}$ of Sakane's model changes due to sympathetic nerve activity and other events such as increased stroke volume that are not associated with such activity. The model therefore needs to be improved for monitoring of sympathetic nerve activity without effects from arterial pressure change.

A number of research groups have proposed evaluation methods involving image inspection for diagnosis of abnormalities in autonomic nervous function. By way of example, Satoh *et al.* evaluated cardiac sympathetic nervous function using ^{123}I-MIBG (^{123}Iodine meta-iodobenzylguanidine) myocardial scintigraphy as a way of discriminating Parkinson's disease from Parkinsonism [27]. Intravenous delivery of concentrated MIBG to myocardial sympathetic nerve endings can be visualized with a conventional

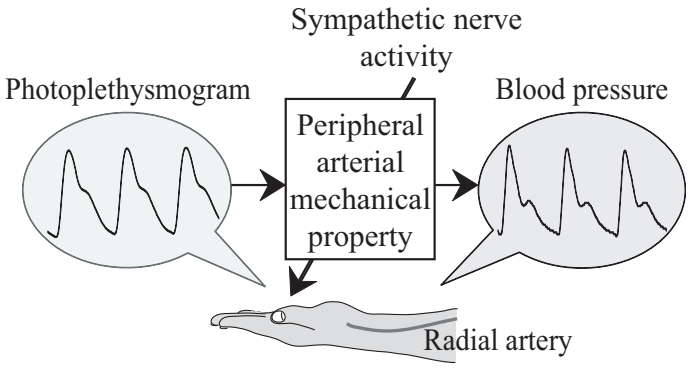

Fig. 1.1: Arterial wall impedance model

gamma camera within 15 minutes of injection, and images of the thorax can be acquired within 4 hours. Cardiac sympathetic nervous function is subsequently assessed in consideration of the ratio of concentrated MIBG in the mediastinum to that in the heart (a metric known as the heart-to-mediastinum (H/M) ratio). The concentration of MIBG here is calculated from the average count of Γ rays per pixel in the regions of interests. The early H/M ratio is measured 15 minutes after MIBG injection, and the late ratio is measured after 4 hours. However, ^{123}I-MIBG myocardial scintigraphy examination involves a high level of risk due to its invasive nature and the need for radioactive medication, which subjects patients to internal exposure. The establishment of a novel and safe examination to allow evaluation of autonomic nervous function in patients with Parkinson's disease and Parkinsonism is therefore needed.

Several approaches are conventionally taken for quantitative evaluation of pain. By way of example, a visual analogue scale (VAS; a common pain intensity metric based on a 100-mm graduated line marked "No pain" on the far left end and "Worst pain imaginable" on the far right) involves measurement of the length from the no-pain point to the point indicated by the patient to represent subjective pain intensity. A numeric rating scale (NRS; another common pain intensity metric scored on an 11-point range

with 0 representing no pain and 10 as the worst pain imaginable) involves the use of numeric values to represent pain intensity [28–30]. Shimazu *et al.* also proposed the Pain Vision method for quantitative evaluation of pain [31]. This approach involves the use of a perceptible stimulus current followed by an initial painful stimulus current. However, these methods are not based on autonomic nerve activity and involve subjective evaluation by the patient. This makes them unsuitable for patients under general anesthesia or those with impaired cognitive function.

1.3 Dissertation Purpose and Outline

Based on the above, evaluation of autonomic nerve activity and autonomic nervous function on the peripheral side can be expected to support evaluation of patient well-being and symptoms. It is also useful in a wide range of applications, including surgical operation assistance, diagnosis support and healthcare. Against such a background, this paper proposes a novel peripheral artery dynamic model that enables estimation of changes in peripheral arterial dynamic characteristics for the evaluation of local autonomic nerve activity. Existing methods of peripheral artery evaluation depend on factors unrelated to sympathetic nerve activity, such as elevations in blood pressure associated with increased stroke volume. Thus, quantitative determination of peripheral artery mechanical characteristics for the evaluation of sympathetic nerve function requires: (i) evaluation to determine the mechanical characteristics of the peripheral arterial wall based on mechanical impedance parameters such as stiffness, viscosity, and inertia; (ii) evaluation of the stiffness parameter, which is considered to influence factors other than sympathetic nerve activity such as the nonlinearity between intravascular pressure and arterial diameter; and (iii) expression of distinctive information on peripheral arteries, i.e., data indicating the effects of veins and accumulation in arte-

rioles. The paper describes a novel mechanical peripheral arterial wall model designed in consideration of the above three conditions, and proposes indices for monitoring of autonomic nerve activity and autonomic nervous function. The proposed indices can be applied to autonomic nerve activity monitoring during surgical operations, support for differential diagnosis between Parkinson's disease and Parkinsonism, and quantitative/objective evaluation of pain.

The paper is organized as follows: Chapter 2 describes a novel technique for estimating the dynamic characteristics of peripheral arterial walls for the evaluation of local autonomic nerve activity at the peripheral side. The proposed model can be used to estimate robust arterial viscoelastic characteristics against blood pressure variations unassociated with autonomic nerve activity and to accurately determine activation of the autonomic nervous system at the peripheral side because the nonlinearity between blood pressure and arterial diameter is considered. In the experiments described here, biological signals of patients under general anesthesia were monitored during surgical operations. The first experiment, in which the subjects lay on a bed that was rolled left and right, showed that the proposed arterial viscoelastic indices do not fluctuate with blood pressure variations unassociated with autonomic nerve activity. The second experiment on ETS, which involved direct stimulation of sympathetic nerves, indicated that the arterial viscoelastic indices calculated from the proposed model support monitoring of the autonomic nervous system at the peripheral side.

Chapter 3 describes a diagnosis support method for Parkinson's disease, which is associated with autonomic nervous function abnormality. The condition has symptoms similar to those of Parkinsonism, but the huge difference in treatment methods for each disease makes it necessary to discriminate between them. The proposed diagnosis support method involves the extraction of feature values based on changes in arterial

viscoelastic characteristics and in the amplitude of photoplethysmograms associated with head-up tilting, and can be used to diagnose normality/abnormality of autonomic nervous function based on disease abnormality markers calculated from a probability neural network. In the experiment described here, the proposed system was applied to head-up tilt testing for patients with Parkinson's disease and Parkinsonism, and was used to make differential diagnosis between the two conditions. The system can also be used to evaluate the autonomic nervous function of patients with Parkinson's disease before and after phototherapy in order to determine therapeutic effects on autonomic nervous function.

Chapter 4 describes a new system that can be used to quantitatively and objectively evaluate human subjective pain intensity. In light of the difficulty of expressing the sensation of pain to those not experiencing it, the system enables quantitative and objective evaluation of pain based on vasoconstriction responses associated with activation of the sympathetic nervous system when pain is felt. This evaluation involves conversion of the peripheral arterial viscoelastic indices detailed in Chapter 2 into subjective pain intensity indicators based on NRS. In the experiment described here, the system was used to measure degrees of pain associated with gradually increasing electrical stimuli. The results indicated that the proposed system can be used to evaluate human pain quantitatively and objectively.

Finally, Chapter 5 concludes the dissertation and outlines a number of future challenges and further work.

Chapter 2

A Log-linearized Peripheral Arterial Viscoelastic Index and Its Application to Endoscopic Thoracic Sympathectomy

2.1 Introduction

This chapter proposes a dynamic model of the peripheral arterial wall. The model allows consideration of the effects of blood pressure changes based on the concept of mechanical impedance and the relationship of nonlinearity between peripheral vascular diameter and intravascular pressure. The results enable evaluation of sympathetic nerve activity around the peripheral part (referred to here simply as the sympathetic nerve). First, verification of the proposed model's validity is described. It was found that the dynamic characteristics of the peripheral artery as calculated using the model do not depend on blood pressure variations. Next, the chapter reports the results of evaluation to determine sympathetic nerve activity in the peripheral part using the proposed model with endoscopic thoracic sympathectomy.

2.2 A Log-linearized Peripheral Arterial Viscoelastic Index

2.2.1 Mechanical Model of a Peripheral Artery

Figure 2.1 shows the proposed mechanical impedance model of the peripheral arterial wall. Here, the wall's characteristics in an arbitrary radial direction are considered, and are shown from changes in force and arterial diameter as follows:

$$\begin{aligned} F(t) &= F_\mu(t) + F_\eta(t) + F_\beta(t) \\ &\approx \tilde{\mu}\ddot{r}(t) + \tilde{\eta}\dot{r}(t) + \tilde{F}_{\tilde{\beta}}(r(t)). \end{aligned} \tag{2.1}$$

Here, $F(t)$ is the normal force acting on the arterial wall at the arbitrary time t; $F_\mu(t)$, $F_\eta(t)$ and $F_\beta(t)$ are the forces originating from inertia, viscosity and stiffness, respectively; and $\tilde{\mu}$ and $\tilde{\eta}$ are the arterial wall inertia and viscosity, respectively. $r(t)$, $\dot{r}(t)$ and $\ddot{r}(t)$ represent the arterial diameter, the rate of change in arterial diameter and the acceleration of change in arterial diameter, respectively. Taking into account the nonlinearity between intravascular pressure and arterial diameter, the force originating from arterial wall stiffness is expressed as $\tilde{F}_{\tilde{\beta}}(r(t))$.

The relationship between blood pressure (BP) and arterial diameter has been extensively investigated in previous experiments [24–26]. For example, Nagasawa *et al.* measured canine intravascular pressure and arterial outside diameter with a femoral artery on an in vitro basis to support examination of the artery's mechanical properties [26]. The results indicated that the canine femoral artery exhibits distensibility in the range of 60 – 180 mmHg. It was also found that the relationship of the ratio of logarithm intravascular pressure to standard pressure and the ratio of arterial outside diameter to arterial outside diameter with standard intravascular pressure are linear. However, in a case with low intravascular pressure, it was observed that the artery stiffened

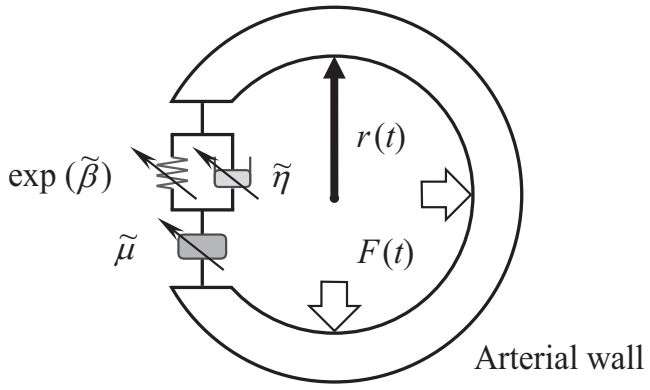

Fig. 2.1: Mechanical impedance model of a peripheral arterial wall

significantly because the blood vessel diameter variation that accompanies increased intravascular pressure became very small [25, 26]. Accordingly, it was assumed in this study that human peripheral arterial characteristics are also nonlinear in the same way as the canine femoral artery in terms of arterial wall mechanical characteristics. Here, the logarithm force originating from arterial stiffness in consideration of the many arterioles in peripheral areas is expressed as follows:

$$\ln\{\tilde{F}_{\tilde{\beta}}(r(t))\} = \tilde{\beta}(r(t) - r_0) + F_{\tilde{\beta}_0} + F_{\tilde{\beta}_{nl}}(r(t)). \tag{2.2}$$

Here, $\tilde{\beta}$ is the arterial stiffness relating to logarithm force, $r(t) - r_0 = dr(t)$ is the arterial diameter change, r_0 is the equilibrium point, and $F_{\tilde{\beta}_0}$ is the constant of the arterial wall. $F_{\tilde{\beta}_{nl}}(r(t))$ is a force originating from stiffness that cannot be log-linearized and accrues when intravascular pressure falls below a certain threshold. Equation (2.2) can be substituted into Equation (2.1) after the exponent is applied on both sides of Equation (2.2), and arterial impedance properties can be expressed as follows:

$$\begin{aligned} F(t) \;\approx\; & \tilde{\mu}\ddot{r}(t) + \tilde{\eta}\dot{r}(t) \\ & + \exp\left\{\tilde{\beta}dr(t) + F_{\tilde{\beta}_0} + F_{\tilde{\beta}_{nl}}(r(t))\right\}. \end{aligned} \tag{2.3}$$

To enable estimation for the impedance parameters of the arterial wall included in

Equation (2.3), the force exerted along the normal direction of the artery $F(t)$ and the variation of the arterial diameter $dr(t)$ need to be measured. Here, for simplification and to support estimation of arterial wall nonlinear impedance parameters, it is assumed that blood pressure $P_b(t)$ is proportional to force $F(t)$:

$$P_b(t) = F(t). \tag{2.4}$$

Meanwhile, as it is difficult to measure vessel diameter changes $dr(t)$ directly *in vivo*, it is assumed that such changes can be approximated using photoplethysmograms (PPGs) measured with a pulse oximeter. PPGs are biological waves whose evaluation is based on the amount of light transmitted through the relatively thin skin on body parts such as fingertips and earlobes. The "photo" part of the name reflects that a pulse oximeter can be used to measure changes in light transmission on the side where the light is applied, which remains constant. PPGs are therefore considered to vary with arterial diameter in the direction of light transmission [32, 33], and the relationship is approximated as follows (see Appendix A):

$$P_l(t) = k_p dr(t) + P_{l0}\ . \tag{2.5}$$

Here, $P_l(t)$ is the photoplethysmogram, k_p is a constant of proportion, and P_{l0} is an offset constant. Equation (2.3) can be expressed using Equations (2.4) and (2.5) as follows:

$$\begin{aligned} P_b(t) &= \mu\ddot{P}_l(t) + \eta\dot{P}_l(t) \\ &\quad + \exp\left\{\beta P_l(t) + P_{b\beta_0} + P_{b\beta_{nl}}(P_l(t))\right\}. \end{aligned} \tag{2.6}$$

Here,

$$\mu = \frac{\tilde{\mu}}{k_p}, \quad \eta = \frac{\tilde{\eta}}{k_p}, \quad \beta = \frac{\tilde{\beta}}{k_p}, \quad P_{b\beta_0} = F_{\tilde{\beta}_0} - \frac{\tilde{\beta}P_{l0}}{k_p}\ ,$$

and

$$P_{b\beta_{nl}}(P_l(t)) = F_{\tilde{\beta}_{nl}}(r(t))$$

represents blood pressure, which cannot be log-linearized and accrues when intravascular pressure decreases. Here, μ, η and β are the inertia, viscosity and stiffness of the arterial wall, respectively. Equation (2.6) represents the log-linearized peripheral arterial viscoelastic model, which can be used to express peripheral arterial dynamic characteristics based on the mechanical impedance parameters of inertia μ, viscosity η and stiffness β.

2.2.2 Algorithm for Estimation of Peripheral Arterial Viscoelastic Indices

The method used to estimate the impedance parameters of inertia μ, viscosity η and stiffness β in 2.2.1 is outlined here. It is difficult to estimate all three parameters at the same time due to the characteristic of $P_{b\beta_{nl}}(P_l(t))$, which cannot be used to express linearity even if it is taken for the logarithm in the element of blood pressure originating with arterial wall stiffness (i.e., the stiffness blood pressure element) in Equation (2.6). Accordingly, parameter estimation is performed in two stages. The procedure for estimating the impedance parameters is described below.

Estimation Method for Inertia Parameter μ and Viscosity Parameter η

The stiffness blood pressure element of Equation (2.6) is approximated in a linear approximate equation using Maclaurin series expansion on the presumption that the higher-order term exceeding the second-order term is sufficiently small as follows:

$$\begin{aligned} &\exp\left\{\beta P_l(t) + P_{b\beta_0} + P_{b\beta_{nl}}(P_l(t))\right\} \\ &\approx \exp\left\{P_{b\beta_0} + P_{b\beta_{nl}}(0)\right\} + \beta_A P_l(t). \end{aligned} \tag{2.7}$$

Here,

$$\beta_A = C_1 \exp\left\{P_{b\beta_0} + P_{b\beta_{nl}}(0)\right\},$$

$$C_1 = \beta + \left.\frac{dP_{b\beta_{nl}}(P_l(t))}{dP_l(t)}\right|_{P_l(t)=0}.$$

Equation (2.6) is therefore approximated as follows:

$$\begin{aligned} P_b(t) &\approx \mu\ddot{P}_l(t) + \eta\dot{P}_l(t) \\ &\quad + \exp\left\{P_{b\beta_0} + P_{b\beta_{nl}}(0)\right\} + \beta_A P_l(t). \end{aligned} \tag{2.8}$$

Here, time t_0 is defined as an arbitrary reference time of the cardiac cycle, such as R wave timing. The dynamic characteristic of the artery at the arbitrary time t can be expressed using Equation (2.8) as follows:

$$dP_b(t) = \mu d\ddot{P}_l(t) + \eta d\dot{P}_l(t) + \beta_A dP_l(t). \tag{2.9}$$

Here $dP_b(t) = P_b(t) - P_b(t_0)$, $d\ddot{P}_l(t) = \ddot{P}_l(t) - \ddot{P}_l(t_0)$, $d\dot{P}_l(t) = \dot{P}_l(t) - \dot{P}_l(t_0)$, and $dP_l(t) = P_l(t) - P_l(t_0)$. μ, η and β_A are estimated using the least-squares method for each heartbeat using Equation (2.9). β_A is an approximation of the stiffness characteristic.

Estimation Method for the Stiffness Parameter β

Substituting μ and η, which are estimated using Equation (2.9), into Equation (2.6) yields an equation that can be used to separate the stiffness blood pressure element from other elements as follows:

$$\begin{aligned} &\exp\left\{\beta P_l(t) + P_{b\beta_0} + P_{b\beta_{nl}}(P_l(t))\right\} \\ &\quad = P_b(t) - \mu\ddot{P}_l(t) - \eta\dot{P}_l(t). \end{aligned} \tag{2.10}$$

Here, taking the exponent on both sides of Equation (2.10), the following is obtained:

$$\begin{aligned} &\beta P_l(t) + P_{b\beta_0} + P_{b\beta_{nl}}(P_l(t)) \\ &\quad = \ln\left\{P_b(t) - \mu\ddot{P}_l(t) - \eta\dot{P}_l(t)\right\}. \end{aligned} \tag{2.11}$$

Accordingly, the dynamic characteristic of the log-linearized stiffness blood pressure element at the arbitrary time t can be expressed as follows using each variation of $P_b(t)$ and $P_l(t)$ at the arbitrary reference time of the cardiac cycle t_0 as well as Equation (2.9):

$$\begin{aligned} &\beta dP_l(t) + P_{b\beta_{nl}}(P_l(t)) - P_{b\beta_{nl}}(P_l(t_0)) \\ &\quad = \ln\left\{\frac{P_b(t) - \mu\ddot{P}_l(t) - \eta\dot{P}_l(t)}{P_b(t_0) - \mu\ddot{P}_l(t_0) - \eta\dot{P}_l(t_0)}\right\}. \end{aligned} \tag{2.12}$$

Here t_0 is the same as the reference time used to estimate μ, η and β_A.

Estimation of the stiffness parameter β is limited to the area where the relationship between the log-linearized stiffness blood pressure element and arterial diameter based on Equation (2.12) is linear: $P_{b\beta_{nl}}(P_l(t)) = P_{b\beta_{nl}}(P_l(t_0))$. When the arterial pressure $P_b(t)$ falls below the level TH and the artery is significantly stiff, the above condition is not fulfilled. The stiffness parameter β is therefore estimated under the area $P_b(t) >$ TH. Here, Equation (2.12) is approximated as follows because $P_{b\beta_{nl}}(P_l(t)) - P_{b\beta_{nl}}(P_l(t_0))$ is equal to 0.

$$\begin{aligned} &\beta dP_l(t)\big|_{P_b(t)>\mathrm{TH}} \\ &\quad = \ln\left\{\frac{P_b(t) - \mu\ddot{P}_l(t) - \eta\dot{P}_l(t)}{P_b(t_0) - \mu\ddot{P}_l(t_0) - \eta\dot{P}_l(t_0)}\right\}\Bigg|_{P_b(t)>\mathrm{TH}}. \end{aligned} \tag{2.13}$$

Stiffness β is estimated for each heartbeat using the least-squares method in Equation (2.13) as well as Equation (2.8).

For the above, the impedance parameters of inertia μ, viscosity η and stiffness β for the arterial wall are estimated using the two-stage method outlined in 2.2.2. In this paper, the stiffness parameter β is proposed as a monitoring index value for peripheral vascular conditions.

2.3 Experiments

First, in order to assess the legitimacy of the proposed model and the proposed impedance estimation algorithm (collectively referred to here as "the proposed method") and determine the index's capacity to reduce the effects of factors causing arterial wall stiffness changes other than sympathetic nervous activity, a supine body roll test [34] was conducted with the subject under general anesthesia. Essentially, to verify the validity of the method proposed in Section 2.2, its approximate accuracy needs to be evaluated using an extracted artery. However, in this study, a minimally invasive procedure for evaluation of the arterial characteristics of a subject was adopted. To verify the usefulness of the proposed method, the first experiment was performed to evaluate impedance parameter changes observed when peripheral blood pressure is forcibly varied during the supine body roll test under general anesthesia. In addition, to evaluate changes in impedance parameters during ETS [4] using the proposed method, a second experiment was performed to measure biological signals and determine the proposed indices.

Figure 2.2 shows the experimental apparatus used for the supine body roll test and ETS. During the experiments, biomedical electrocardiograms (ECGs), invasive radial arterial blood pressure values and PPGs of the thumb were simultaneously measured at 125 Hz using a bedside monitor (BSS-9800, Nihon Kohden Corp., Tokyo, Japan) and computerized via Transmission Control Protocol (TCP). Figure 2.3 shows measured ECGs, BP values and PPGs. The proposed indices were estimated using measured biological signals. As these signals were affected by various artifacts such as light and mechanical stimulation of the patient's hand, they were preprocessed using digital filters. The ECGs were filtered using a second-order IIR band-pass filter (14 – 28 Hz), and the BP values and PPGs were filtered using a second-order IIR band-pass filter

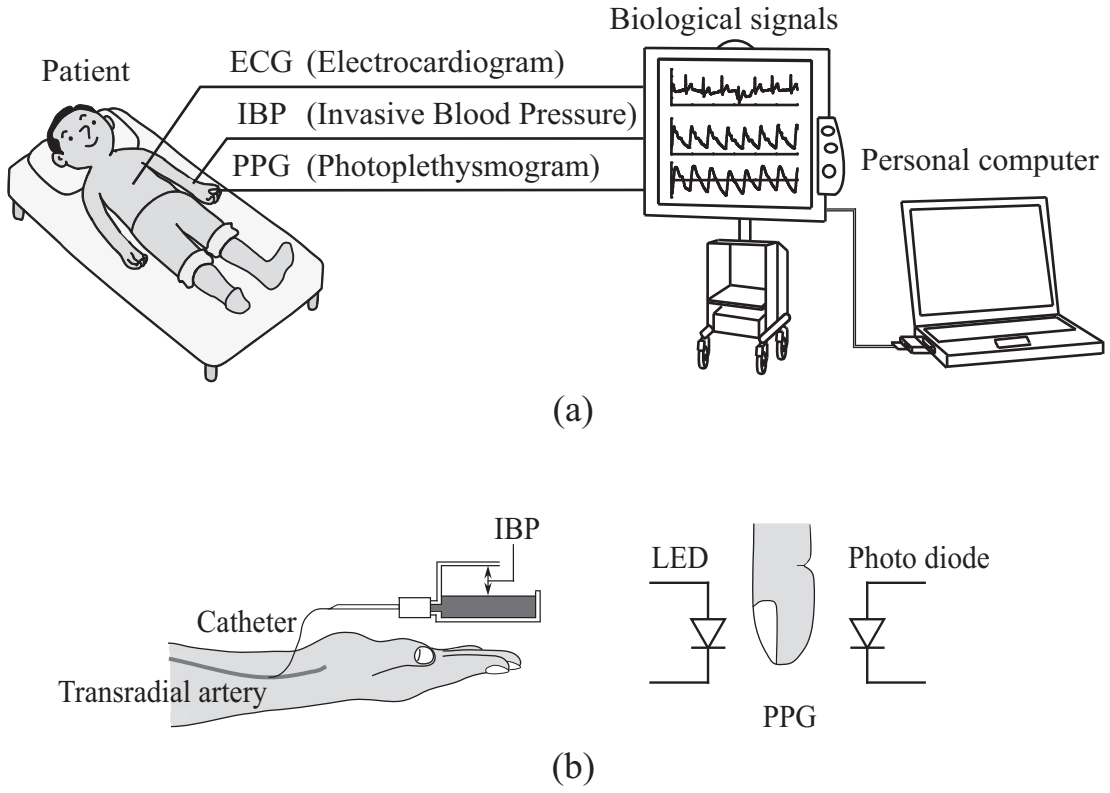

Fig. 2.2: Experimental set-up: (a) experimental instruments: (b) measurement of invasive blood pressure with a catheter from the radius artery at the wrist, and measurement of photoplethysmograms with a pulse oximeter from the thumb

(0.3 – 10 Hz). Parameters with coefficients of determination of 0.95 or more between the measured and presumed blood pressures were used to assess patient conditions. Outliers caused by disturbances such as external light and vibration applied to the patient's hands were also excluded before calculation of the proposed index. Here, the threshold level of Equation (2.13) is defined as the mean blood pressure (MBP) for each heartbeat, and is updated after each heartbeat.

In line with the Declaration of Helsinki, informed consent was secured from all study subjects before the experiments were performed, and the approval of the Hiroshima University Ethics Committee was also obtained.

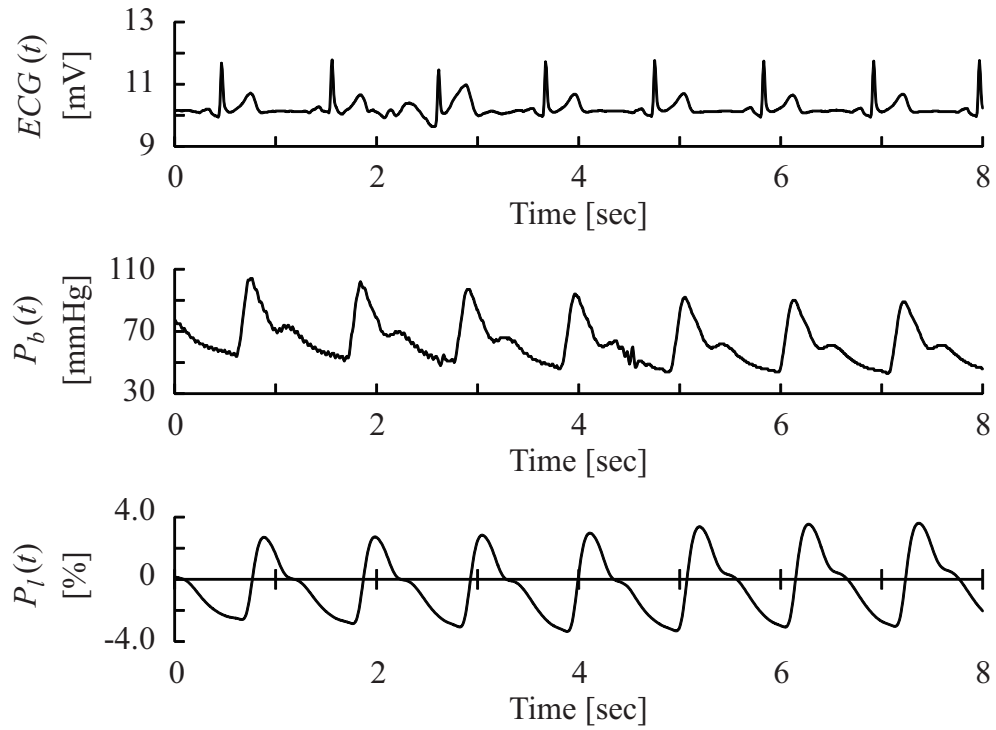

Fig. 2.3: Example of measured biological signals: ECGs, BP values and PPGs

2.3.1 Supine Body Roll Test

This experiment was conducted to measure BP values and PPGs associated with intravascular pressure variations resulting from changes in the target part's position [34], with the fingertip being moved up and down on the basis of the heart's height. For six patients, invasive radial arterial pressure values and photoplethysmograms of the left thumb were simultaneously measured during the supine body roll test. The patients under general anesthesia were laid supine on an operating table, which was then inclined to the left by 10 – 15 degrees and tilted twice alternately (Figure 2.4). The test was performed on patients under general anesthesia and before operation because the effects of vasoconstriction resulting from mental stress can also have some influence. The experiment verified two points in particular, as outlined below.

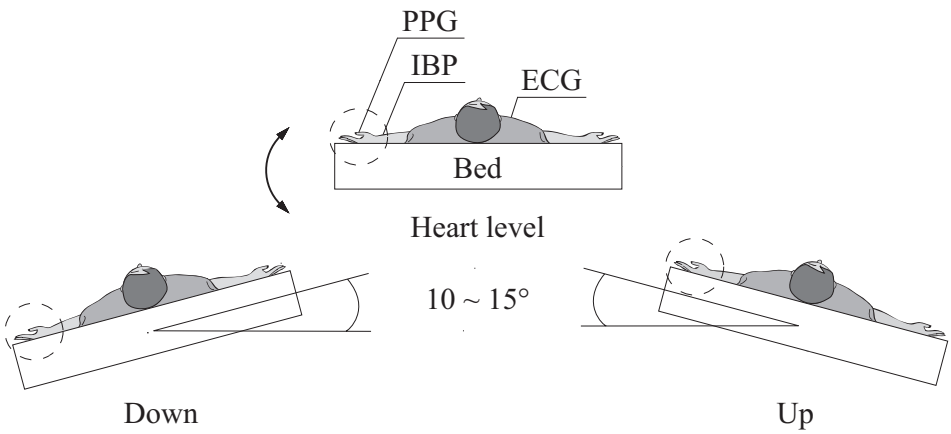

Fig. 2.4: Supine body roll test

Validity of the Proposed Method

The proposed method's validity was verified on the basis of the following two points using biological signals measured with the subjects at rest before the supine body roll test: (i) the proposed model can be used to express the mechanical properties of the peripheral vascular system with stiffness, viscosity and inertia; (ii) the proposed method can be used to estimate the stiffness parameter in the area where the relationship between the log-linearized stiffness blood pressure element and the arterial diameter is linear.

In (i), blood pressure elements were first classified as follows: (a) measured BP; (b) blood pressure element originating from arterial wall viscosity (referred to as the viscosity blood pressure element) subtracted from measured BP; and (c) blood pressure element originating from arterial wall inertia (referred to as the inertia blood pressure element) and the viscosity blood pressure element subtracted from measured BP. Next, the area of the Lissajous curve drawn from the PPG and (a), (b) and (c) was calculated, and the reduced ratios between (a) and (b) and between (b) and (c) were compared after the measured BP was normalized. The results showed the mean $\pm$ standard deviation.

Welch's t-test was used to determine the significance of the differences between (a) and (b) and between (b) and (c) after the application of Bonferroni correction, and differences were considered to be significant when results showing $p < 0.05$ were seen.

In (ii), verification was performed to determine whether the quality and integrity of the proposed method remained if indices varied with arm position changes; that is, the aim was to establish whether the Lissajous curve between the log-linearized stiffness blood pressure element and PPG produces a small area and is nearly linear in parts with more than the threshold TH.

Effectiveness of the Proposed Method

To support discussion of the reduced state of the proposed method for the influence of stiffness changes caused by the absence of sympathetic nerve activity, stiffness estimated with the proposed method [23] was compared to that estimated with the conventional method shown in Equation (1.1). Variations in both stiffness parameters β and $\tilde{K}$ were normalized by the average of 30 sec at rest, and those in the normalized parameters were compared with data from 20 sec in the down and up directions, respectively. Statistical analysis was performed using Welch's two-tailed t-test, and the level of significance was set at $p < 0.05$.

2.3.2 Endoscopic Thoracic Sympathectomy

ETS is an operation performed under anesthesia for patients with hyperhidrosis [4]. The sympathetic trunk is a thin, white sinewy bundle of nerve fibers running along the spine of the thorax. It stimulates arterial contraction and sweat generation on the palms and in the armpits [35]. In ETS, the sympathetic trunk is blocked with a clip to control sweating [4]. The proposed method was applied to support sympathetic nerve activity evaluation using biological signals measured during the T3 level of ETS on the

right and left parts of the thorax for 15 patients (5 males and 10 females; mean age ± S.D.: 23.7 ± 9.0 yrs). BP values were measured with an arterial line inserted from the right radial artery, and PPGs were measured from the thumb of the right hand.

The sympathetic nervous condition at the measurement site changed from moment to moment depending on the surgical situation. First, ETS was performed to clip the right thoracic sympathetic trunk [36]. At this point, the stiffness parameter β in the vicinity of the measurement area (the right hand) rose with neural stimulus in line with sympathetic nerve search, and the stiffness parameter β attenuated after the nerve was clipped because stimulation was cut off. Next, the sympathetic trunk on the left side was clipped; that on the right had been already clipped at this point. When clipping of the sympathetic trunk on the right side is successful, the stiffness parameter β is not expected to change because stimuli do not propagate from left to right. To check such changes of the stiffness parameter β in association with operation events, the value was normalized using the corresponding mean of values measured with the patient at rest, and focus was placed on a normalized stiffness β of 20 seconds as follows:

- rt-con: 400 seconds before the beginning of search of the right thoracic sympathetic trunk for blocking
- rt-stim: 200 seconds before blocking of the right thoracic sympathetic trunk
- rt-post: 200 seconds after blocking of the right thoracic sympathetic trunk

Welch's t-test was used to determine the significance of differences between the stiffness parameter β of rt-con and that of rt-stim and between that of rt-stim and that of rt-post after the application of Bonferroni correction for each β, and differences were considered significant when results showing $p < 0.05$ were seen. The stiffness parameter β was also compared with the stiffness parameter $\tilde{K}$ for each event.

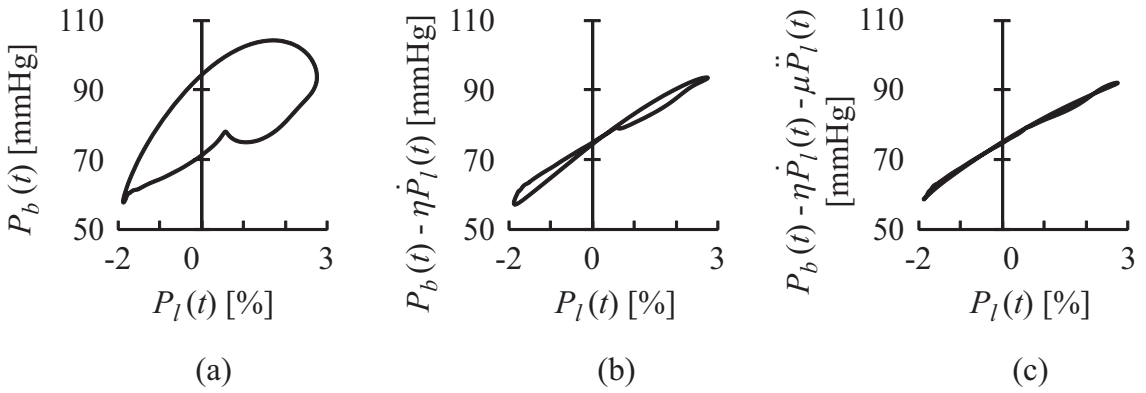

Fig. 2.5: Example of Lissajous curves for blood pressure values vs. measured $P_l(t)$: (a) $P_l(t)$ vs. $P_b(t)$, (b) $P_l(t)$ vs. $P_b(t) - \eta\dot{P}_l(t)$, (c) $P_l(t)$ vs. $P_b(t) - \eta\dot{P}_l(t) - \mu\ddot{P}_l(t)$

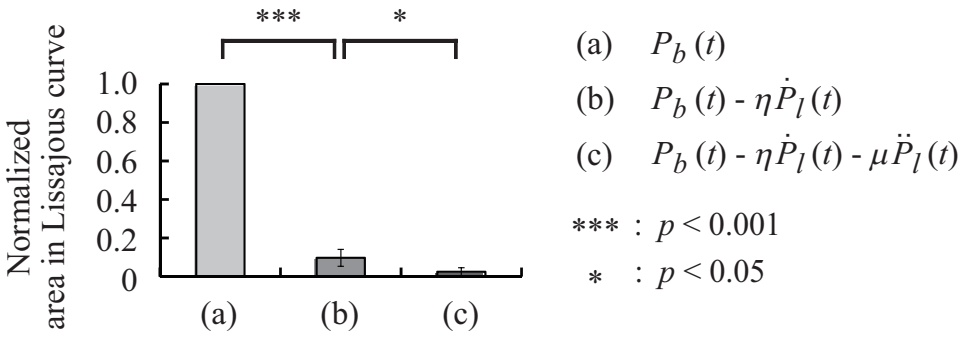

Fig. 2.6: Comparison of normalized areas in Lissajous curves

2.4 Results

2.4.1 Supine Body Roll Test

Figure 2.5 shows an example of the Lissajous curves obtained from Patient A. The horizontal axis represents the photoplethysmogram $P_l(t)$. The vertical axis of (a) represents blood pressure, that of (b) represents the viscosity blood pressure element subtracted from measured BP, and that of (c) represents the viscosity and inertia blood pressure elements subtracted from measured BP. Figure 2.6 shows the average of the normalized Lissajous curve area after each patient had rested for 20 beats. Figures 2.6

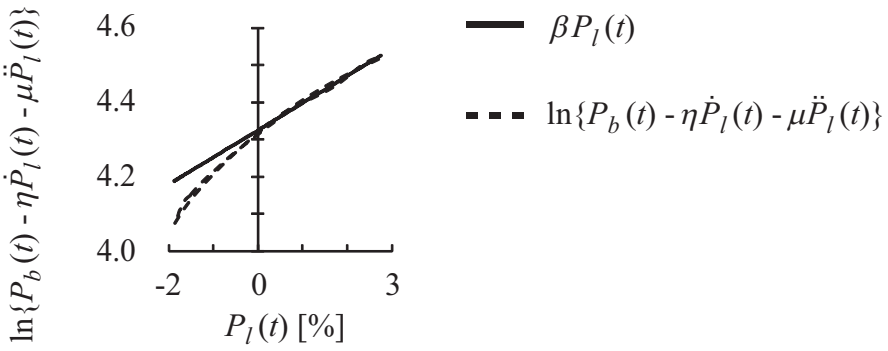

Fig. 2.7: Relationship between stiffness-related blood pressure and measured $P_l(t)$

(a), (b) and (c) correspond to Figs. 2.5 (a), (b) and (c). Here, the areas of the Lissajous curves in Figs. 2.6 (a), (b) and (c) are 1, 0.097 ± 0.044 and 0.024 ± 0.021, respectively. It can be concluded that the blood pressure element eliminated from viscosity blood pressure and inertia blood pressure significantly decreased after elimination ((a) vs. (b): $p = 5.913 \times 10^{-8}$; (b) vs. (c): $p = 1.601 \times 10^{-2}$).

Figure 2.7 shows an example of the Lissajous curve for the photoplethysmogram $P_l(t)$ and a log-linearized stiffness blood pressure element (broken line), and for the photoplethysmogram $P_l(t)$ and a stiffness blood pressure element based on the proposed method (solid line). In Figure 2.7, the broken line corresponds relatively closely to the solid line, and is linear in the area where the log-linearized stiffness blood pressure element was higher than or equal to the threshold TH. However, the broken line curves and differs significantly from the solid line in the area where the log-linearized stiffness blood pressure element was lower than or equal to the threshold TH. The difference between the two lines corresponds to the nonlinear characteristic $P_{b\beta_{nl}}(P_l(t))$ of Equation (2.6). The mean square errors between the broken and solid lines for the same beats are shown in Figure 2.6. Figure 2.8 shows the mean square errors between the lines for the average of all patients in the area where the log-linearized stiffness blood pressure

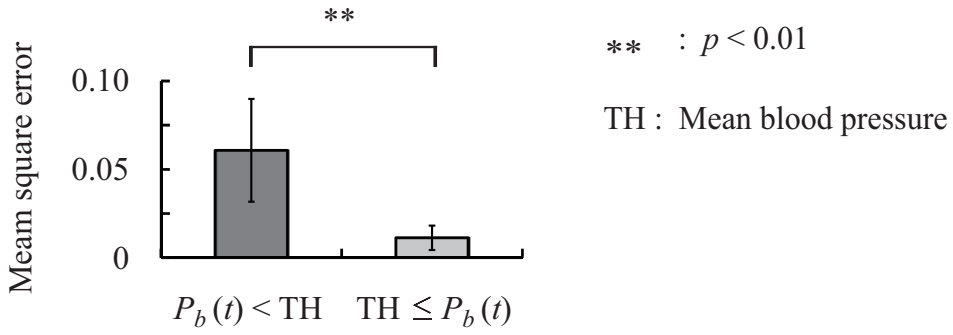

Fig. 2.8: Mean square error between the predicted stiffness blood pressure element $\beta P_l(t)$ and the logarithm of residual blood pressure in $P_b(t) - \eta \dot{P}_l(t) - \mu \ddot{P}_l(t)$

element was higher than or equal to and lower than the threshold TH, respectively. The mean square error was $6.07 \times 10^{-2} \pm 2.91 \times 10^{-2}$ and $1.13 \times 10^{-2} \pm 0.69 \times 10^{-2}$ in the area where the log-linearized stiffness blood pressure element was higher than or equal to the threshold TH and less than the threshold TH, respectively, indicating a significant difference between the two areas ($p = 7.88 \times 10^{-3}$).

Figure 2.9 shows the measured and estimated data from the supine body roll test for Patient A. The figure plots the left arm position with the inclination of the operating table, mean blood pressure (MBP), pulse pressure (PP), PPG amplitude (which is the difference between the maximum $P_l(t)$ and minimum $P_l(t)$ per beat (PPG_a)), the proposed stiffness parameter β and the conventional stiffness parameter $\tilde{K}$. Figure 2.9 indicates a significant response of MBP and PPG_a to the changing inclination of the operating table. Meanwhile, PP was stable in comparison to the variation of MBP. Correspondingly, the proposed stiffness parameter β was approximately constant, whereas the conventional stiffness parameter $\tilde{K}$ changed significantly with body rotation. Figure 2.10 shows the normalized stiffness parameters β and $\tilde{K}$ with the patient at rest in the down and up positions. The stiffness parameters β and $\tilde{K}$ were 1.055 ± 0.023 and 1.240 ± 0.041 in the down position, and 0.960 ± 0.030 and

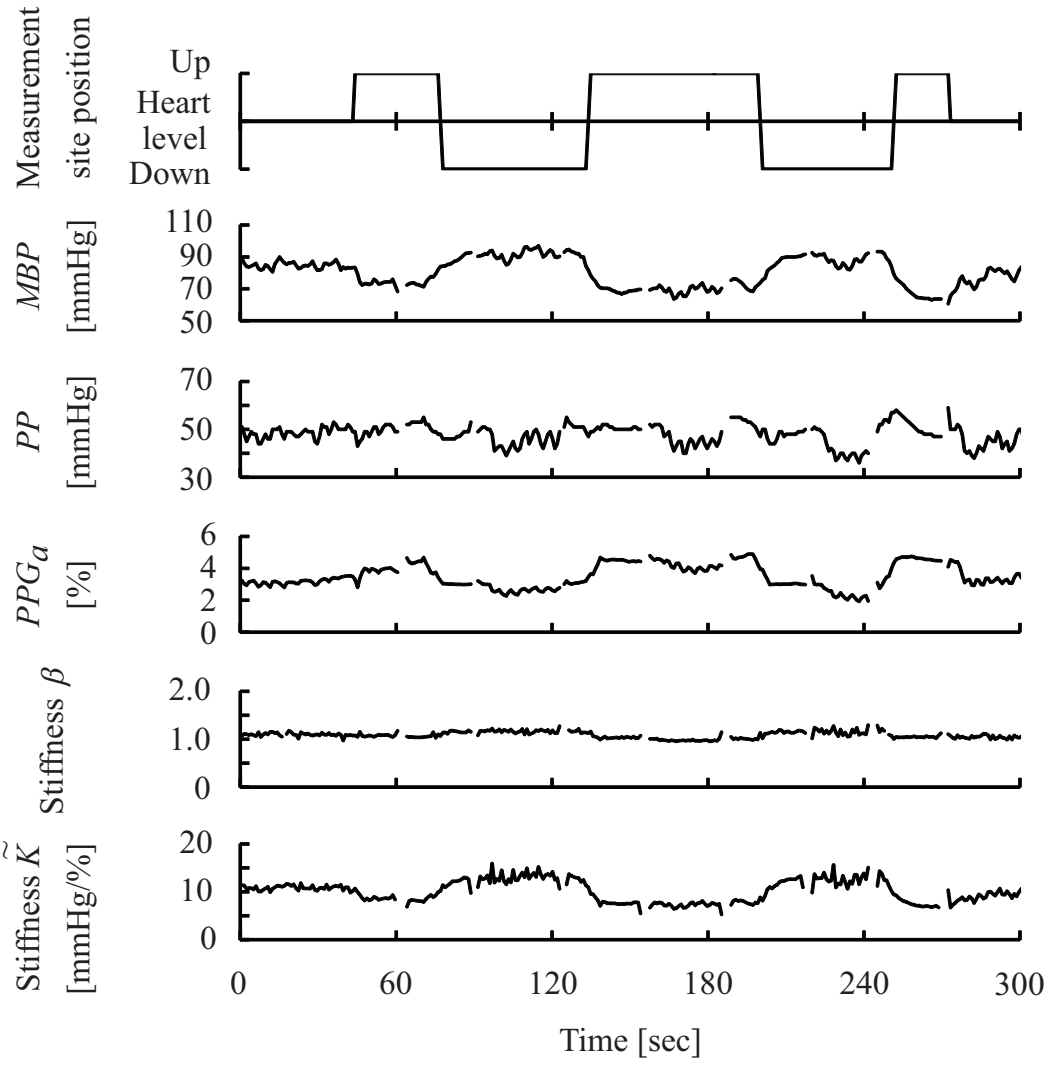

Fig. 2.9: Measured biological signals and estimated results for the stiffness parameters of the peripheral arterial wall during the supine body roll test (Patient A)

0.753 ± 0.035 in the up position, respectively. These results indicate a significant difference between the two values in the down and up positions (down: $p = 1.187 \times 10^{-5}$; up: $p = 8.975 \times 10^{-7}$).

2.4.2 Endoscopic Thoracic Sympathectomy

Figure 2.11 shows typical ETS data retrieved from Patient G. The figure plots mean

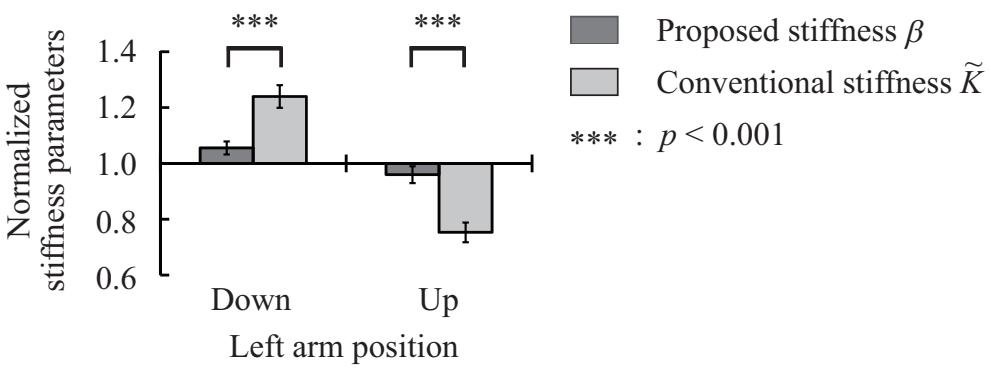

Fig. 2.10: Comparison of normalized stiffness parameters observed during the supine body roll tests

blood pressure (MBP), pulse pressure (PP), PPG amplitude (PPG_a), the proposed stiffness parameter β and the conventional stiffness parameter $\tilde{K}$ [23]. The light shaded area corresponds to the period during stimulation applied to locate the right thoracic sympathetic nerve, and the dark shaded area corresponds to the period during that for the left one.

Figure 2.12 shows averages of the proposed stiffness parameter β and the conventional stiffness parameter $\tilde{K}$ for rt-con, rt-stim and rt-post. The stiffness parameter β was 1.028 $\pm$ 0.028, 7.000 $\pm$ 2.785 and 1.173 $\pm$ 0.0.157 in the order of rt-con, rt-stim and rt-post, and the stiffness parameter $\tilde{K}$ was 1.035 $\pm$ 0.072, 8.001 $\pm$ 3.235 and 1.233 $\pm$ 0.276 in the same order. These results indicate a significant difference between rt-con and rt-stim for the stiffness parameters β and $\tilde{K}$, and between rt-stim and rt-post ($p < 0.001$).

It is also seen that clipping of the right thoracic sympathetic trunk succeeded when PPG_a was stable or increased regardless of the rise in MBP seen during blocking of the left thoracic sympathetic nerve. The stiffness parameter β for lt-con (lt-con: 200 seconds before the beginning of stimulation applied to locate the left thoracic sympathetic trunk for blocking) and lt-stim (lt-stim: 200 seconds before the blocking of the

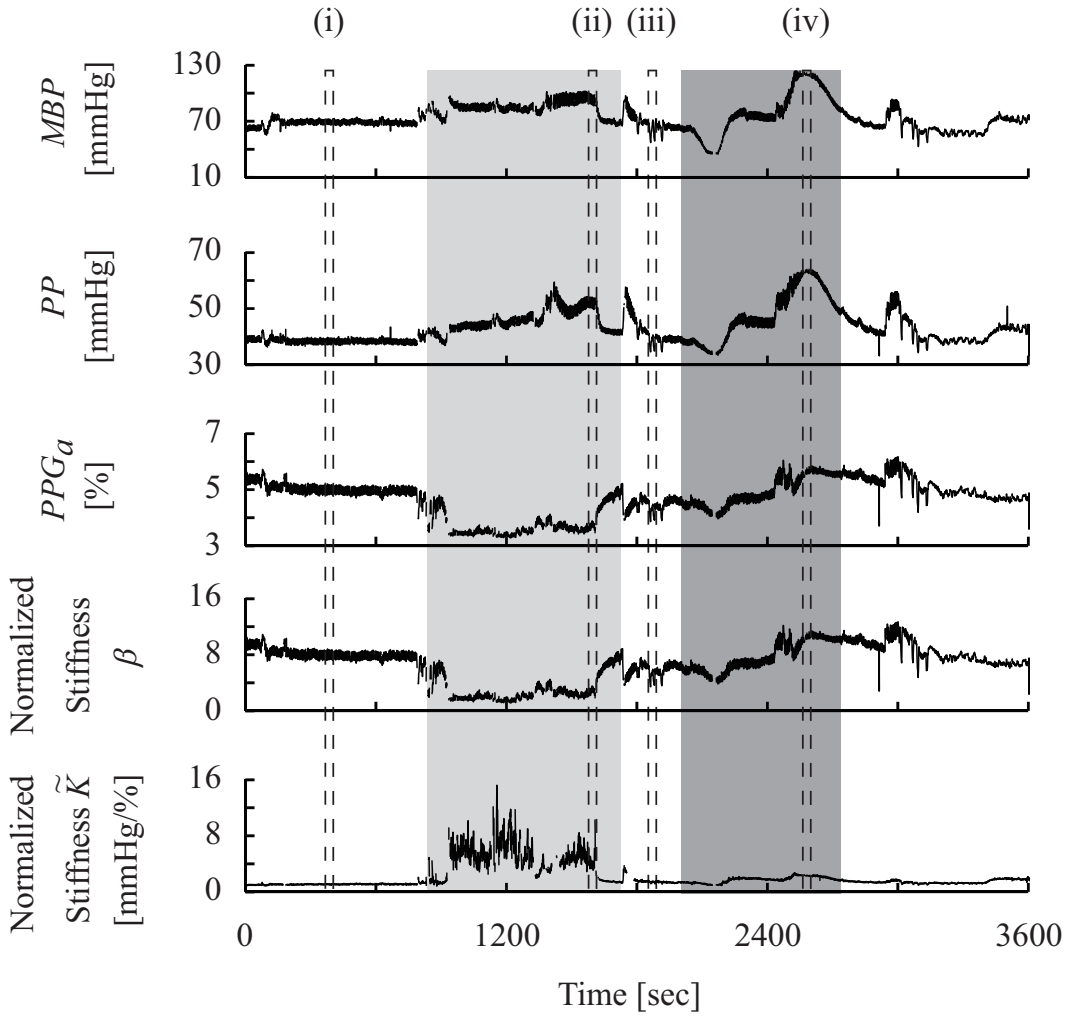

Fig. 2.11: Measured biosignals and estimated results for the stiffness parameters of the peripheral arterial wall in endoscopic thoracic sympathectomy (Patient A): (i) rt-con, (ii) rt-stim, (iii) rt-post and lt-con and (iv) lt-stim

left thoracic sympathetic trunk) were then compared with the stiffness parameter $\tilde{K}$ of four patients for whom clipping of the right thoracic sympathetic trunk was considered successful. Figure 2.13 shows that the proposed stiffness parameter β for lt-con was 1.266 ± 0.183, while that for lt-stim was 1.413 ± 0.313. In addition, the conventional stiffness parameter $\tilde{K}$ for lt-con was 1.355 ± 0.368, while that for lt-stim was 1.989 ± 0.444. Here, it should be noted that blood pressure variations in some patients were

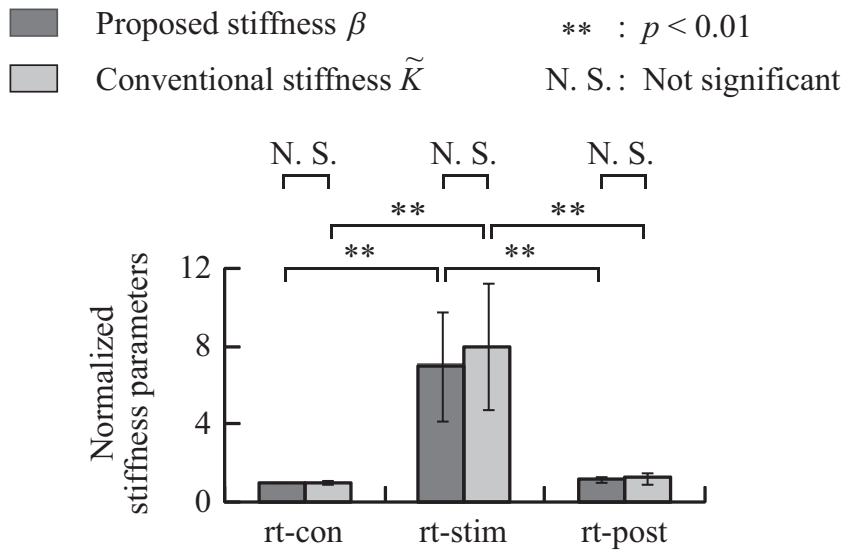

Fig. 2.12: Comparison of normalized stiffness parameters observed in endoscopic thoracic sympathectomy

Table 2.1: T-test of normalized stiffness parameters observed during endoscopic thoracic sympathectomy

Comparison		p-value
Target	Groups	
β	rt-con vs. rt-stim	$p < 0.001$
	rt-stim vs. rt-post	$p < 0.001$
$\widetilde{K}$	rt-con vs. rt-stim	$p < 0.001$
	rt-stim vs. rt-post	$p < 0.001$

Comparison		p-value
Target	Groups	
rt-con	β vs. $\widetilde{K}$	N. S.
rt-stim	β vs. $\widetilde{K}$	N. S.
rt-post	β vs. $\widetilde{K}$	N. S.

N. S.: Not significant

not associated with blocking of the left thoracic sympathetic trunk because the effects of anesthesia vary by individual. The results and Table 2.2 indicate a significant difference between the conventional stiffness parameter $\tilde{K}$ for lt-con and that for lt-stim, and between the conventional stiffness parameter β and $\tilde{K}$ for lt-stim ($p < 0.05$).

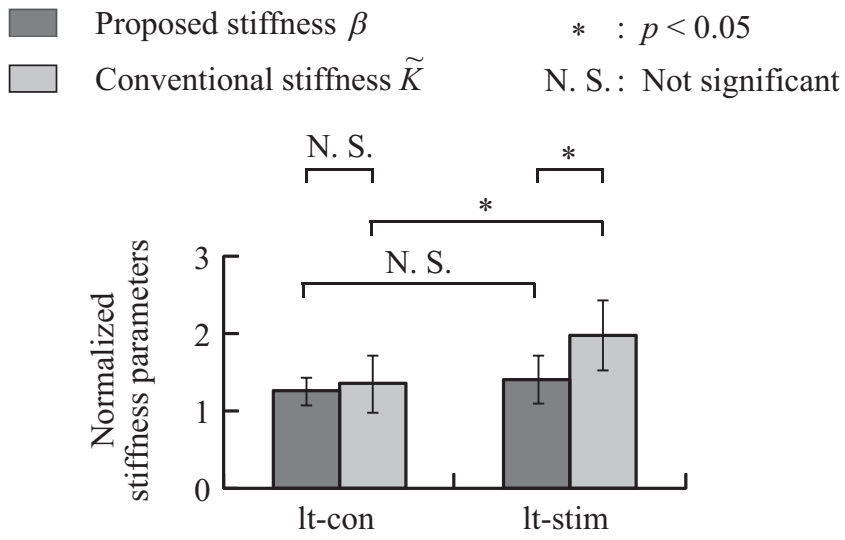

Fig. 2.13: Comparison of normalized stiffness parameters observed before and during left-side endoscopic thoracic sympathectomy

Table 2.2: T-test of normalized stiffness parameters observed before and during left-side endoscopic thoracic sympathectomy

Comparison		p-value
Target	Groups	
β	lt-con vs. lt-stim	N. S.
$\widetilde{K}$	lt-con vs. lt-stim	$p < 0.05$

Comparison		p-value
Target	Groups	
lt-con	β vs. $\widetilde{K}$	N. S.
lt-stim	β vs. $\widetilde{K}$	$p < 0.05$

N. S.: Not significant

2.5 Discussion

Figures 2.5 and 2.6 indicate that the area of the Lissajous curve between PPG and the blood pressure element, which was eliminated from the viscosity blood pressure element and inertia blood pressure element, decreased after elimination. The relationship between PPG and BP shows a hysteresis characteristic because the measured blood pressure elements were included in the viscosity blood pressure element and the inertia blood pressure element. The peripheral arterial dynamics were thus expressed

using inertia as well as stiffness and viscosity.

Figures 2.7 and 2.8 indicate that the log-linearized stiffness blood pressure element is characterized by both linearity and nonlinearity. That in the nonlinear area is smaller than that in the linear area. This indicates that the force applied to the artery in association with diastolic blood pressure is inertial, and an artery subjected to this force cannot be treated as a vasodilating entity. For accurate evaluation of arterial wall stiffness without enucleation of the artery, the stiffness parameter should therefore be estimated only for the area from which linearity between the PPG and the log-linearized stiffness blood pressure element is determined.

Figures 2.9 and 2.10 indicate that the ratio of change in the normalized proposed stiffness parameter β calculated from the proposed model is significantly lower than that of the normalized conventional stiffness parameter $\tilde{K}$ calculated from the previous model for the supine body roll test. As the patients in this test were under general anesthesia, sympathetic vasoconstriction did not occur due to the absence of mental strain [37, 38]. Application of the proposed method thus reduced vascular stiffness changes associated with intravascular pressure variations. The contributing factor of stiffness change without sympathetic nerve activity incorporates vascular diameter regulatory mechanisms such as myogenic response [39]. In future work, the authors plan to consider this contributing factor in more detail.

Figure 2.11 indicates that the proposed stiffness parameter β rapidly responded to stimulation applied to locate the sympathetic nerve between rt-con and rt-stim. This suggests that the parameter increased because nerve stimulation resulted in peripheral artery constriction [40]. Additionally, changes in the proposed stiffness parameter β between rt-stim and rt-post were suppressed after clipping of the right thoracic sympathetic nerve. Thus, the results suggest that the peripheral arteries quickly took on a

relaxed state in contrast to their previously tense condition. It is notable that the estimated stiffness parameter β did not markedly increase around $t = 2{,}550$ seconds during lt-stim (Fig. 2.11 (iv)), while MBP was seen to increase. At the same time, both the pulse pressure PP and the PPG amplitude PPG_a variation increased. It was therefore concluded that ETS on the right side was successful. Figure 2.11 indicates that the conventional stiffness parameter $\tilde{K}$ (for which the nonlinear relationship between blood pressure and vessel diameter is not considered) changed during left-side ETS, while the proposed stiffness parameter β (for which the nonlinear relationship between intravascular pressure and arterial diameter is considered) did not. This strongly suggests that the proposed stiffness parameter β can be estimated for sympathetic nerve activity only without the effects of variations in peripheral arterial stiffness dependent on intravascular pressure.

2.6 Concluding Remarks

This Chapter outlines an arterial mechanics model based on mechanical impedance in which intra-arterial pressure dependency specific to peripheral arteries is considered, and proposes a log-linearized peripheral arterial viscoelastic index that can be used to clarify sympathetic activity. The validity and effectiveness of the proposed index were considered in two experiments. In the supine body roll test, the validity of the model and the related estimation method were demonstrated based on Lissajous curves of blood pressure vs. plethysmograms and the high correlation between estimated and actual blood pressure values. For changes in arm elevation during peripheral artery monitoring, the proposed indicator reduced the effects of intra-arterial pressure better than the conventional model according to comparison of changes in the stiffness $\tilde{K}$ of the conventional arterial mechanics model and the stiffness β of the proposed

indicator. In endoscopic thoracic sympathectomy, stiffness β varied in response to surgical treatment, and acute sympathetic nerve activity was accurately determined. Further, immediately after the right sympathetic nerve was blocked, no reaction was observed in stiffness β monitored in the right sympathetic nerve during stimulation of the left sympathetic nerve, demonstrating that stiffness β can be used to evaluate local sympathetic nerve activity.

Chapter 3

Diagnosis System for Parkinson's Disease Using a Head-up Tilt Test

3.1 Introduction

This chapter outlines a novel peripheral autonomic nervous function-related method for Parkinson's disease (PD) diagnosis using a head-up tilt test (HUT) [17] without reference to electrocardiograms. The technique involves the extraction of eight feature values from photoplethysmogram (PPG) signals, systolic blood pressure (SBP) and diastolic blood pressure (DBP) measured every minute during HUT. It enables differential diagnosis between PD and Parkinsonism (Pism) based on an autonomic nervous function abnormality marker identified from the learning of biological signal patterns using the type of neural network (NN) often adopted in pattern classification for biological signals. This chapter describes the results of differential diagnosis for PD/Pism based on this marker and outlines the results of verification to determine improvements in autonomic nervous function between the stages before and after phototherapy [41].

3.2 Diagnosis System for Autonomic Nervous Function

When a person moves from a recumbent position into a standing position, barore-

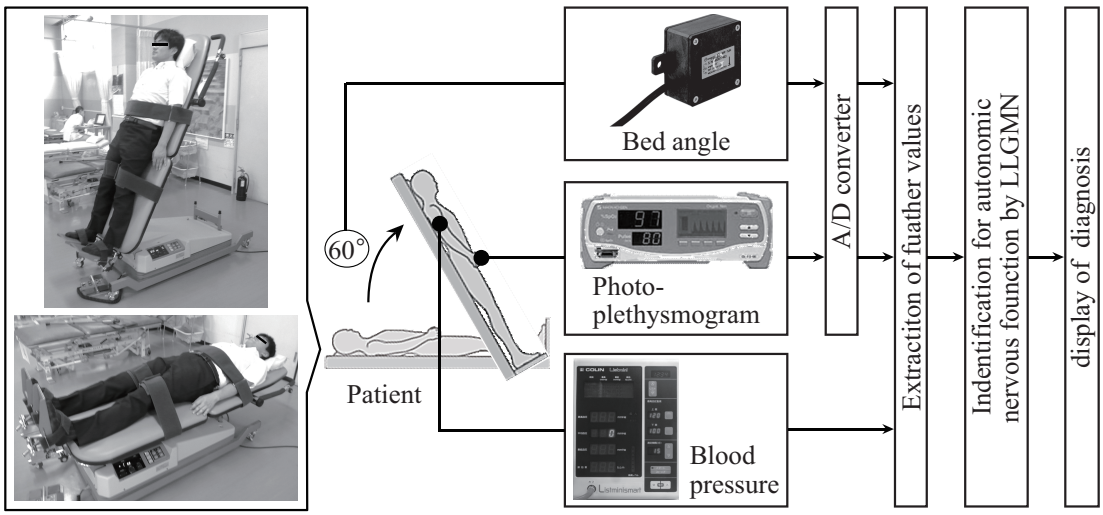

Fig. 3.1: Overview of the proposed system

ceptors in the carotid sinus sense a fall in cerebral blood pressure because blood in the upper body moves to the lower limbs due to the force of gravity. Lower-limb vascular resistance then increases due to the baroreceptor reflex arc function because the sympathetic nervous system is fully active when autonomic nervous function is normal. This function causes blood that has descended under the force of gravity to return to the upper body, thereby maintaining blood pressure and preventing loss of consciousness. Meanwhile, the sympathetic nervous system is not fully active when autonomic nervous function is abnormal [1]. This condition prevents the increased blood volume in the lower limbs from returning to the upper body, and especially to the brain, which may cause orthostatic hypotension. Here, the author proposes a novel method for autonomic nervous function evaluation using biomedical signals during HUT based on the above biological reaction.

Figure 3.1 shows the proposed examination system. In the experiment performed for validation, the subject was instructed to assume a supine position at rest on an electric tilt table at an angle of 0 degrees from the horizontal for at least 10 minutes

(referred to as the first supine position). The tilt was then changed to 60 degrees, and the patient was asked to maintain a resting position (referred to as the standing position). The tilt was subsequently changed back to 0 degrees, and the patient was asked to maintain a resting position for at least five minutes (referred to as the second supine position). In the measurement part of the proposed system, index finger PPGs are measured using a pulse oximeter (OLV-3100, Nihon Kohden Corp., Tokyo, Japan) and the slope angles of the tilt table are measured using a potentiometer (WR-7UH, Midori Precisions, Tokyo, Japan). Both signals are stored at 500 Hz using an analog/digital converter (CSI-360116, Interface Corp., Hiroshima, Japan). The patient's SBP and DBP are also measured every minute using a sphygmomanometer (BP-8800S, Omron Colin, Tokyo, Japan). All measured data are input to a PC.

In the feature value extraction part, the proposed feature values are calculated from the measured PPGs and blood pressure (BP) values. If the sympathetic nervous system is not fully active when the subject is in the standing position, the blood vessels may not stiffen due to the reduced contractile force of vascular smooth muscle associated with sympathetic nerve function [1]. The author therefore proposes a method for evaluating autonomic nervous function based on calculation of extracted PPG amplitudes and estimation of arterial wall stiffness among the first supine position, the standing position and the second supine position. First, feature values were defined based on the following aspects of the calculated PPG amplitudes: x_1: the rate of change in PPG amplitude between the standing position and the first supine position (standing position/first supine position); x_2: the rate of change in PPG amplitude between the second supine position and the standing position (second supine position/standing position); x_3: the rate of change in PPG amplitude between the second supine position and the first supine position (second supine position/first supine position); and x_4:

the slope of the regression line of PPG amplitude recorded while the gradient of the tilt table was increased. Next, feature values were calculated from changes in arterial stiffness. The characteristics of peripheral arterial dynamics derived from sympathetic nerve activity may be presumed to be as follows:

$$\begin{aligned} P_b(t) &= \mu\ddot{P}_l(t) + \eta\dot{P}_l(t) \\ &\quad +\exp\left\{\beta P_l(t) + P_{b\beta_0}\right\} \end{aligned} \tag{3.1}$$

Here, $P_b(t)$, $P_l(t)$, $\dot{P}_l(t)$ and $\ddot{P}_l(t)$ are blood pressure, the arterial diameter, the velocity of change in arterial diameter, and the acceleration of change in arterial diameter, respectively, all measured at the arbitrary time t. $P_{b\beta_0}$ is the standard blood pressure. μ, η and β are the arterial wall's inertia, viscosity and stiffness, respectively. Here, time is limited to t_s for SBP and t_d at DBP for each beat for simplification. $\dot{P}_l(t)$ is then equal to zero because arterial dilation is at both its maximum and minimum during a beat. In addition, it is assumed that $\ddot{P}_l(t)$ is negligibly small. Accordingly, Equation (3.1) can be expressed as follows:

$$P_b(t) = \exp\left\{\beta P_l(t) + P_{b\beta_0}\right\} \qquad (t = t_s, t_d) \tag{3.2}$$

After the logarithm is taken on both sides of Equation (3.2), the stiffness parameter β is estimated for each heartbeat using the substitution equations of time t_s and t_d. Definition of the feature values here was based on the following aspects of the calculated stiffness parameter β: x_5: the rate of change in the stiffness parameter β between the standing position and the first supine position (standing position/first supine position); x_6: the rate of change in the stiffness parameter β between the second supine position and the standing position (second supine position/standing position); x_7: the rate of change in the stiffness parameter β between the second supine position and the first supine position (second supine position/first supine position); and x_8: the slope of

the regression line of the stiffness parameter β recorded while the gradient of the tilt table was increasing. The period for evaluating the first supine position was defined as the three minutes just before the tilt table started to rise due to the potential for an increase in the subject's autonomic nerve activity caused by factors unassociated with disease (such as sleepiness) after the start of the examination; that for the standing position was the three minutes immediately after the tilt table finished rising; and that for the second supine position was the three minutes immediately after the tilt table became horizontal again. In this way, the time lengths used for analysis were uniform.

In the pattern identification part, pattern classification was conducted using the extracted evaluation feature values. Linear discriminant analysis and NNs are often used in pattern identification for biological signals. Previously, Tsuji *et al.* proposed a log-linearized Gaussian mixture network (LLGMN) [42] as a feed-forward probabilistic NN based on the mixture model and the log-linear model of the probability density function. The proposed system involves the use of the LLGMN for PD diagnostics. Figure 3.2 shows the network structure of the LLGMN. Here, $\oslash$ is an identity output unit. The LLGMN consists of an input layer, a middle layer and an output layer. The latter incorporates two units that output posteriori probabilities of normal/abnormal autonomic nervous function classes. The log-linearized Gaussian mixture model is based on machine learning using teacher signals. Such learning with backpropagation allows the updating of weight values to minimize Kullback-Leibler information. The proposed system outputs posteriori probabilities of these classes to the input of signals using the networks learned based on teacher signals (see Appendix B). The posteriori probability of abnormal autonomic nervous function, which is referred to as the autonomic nervous function abnormality marker, is proposed as an index for autonomic nervous function diagnostics.

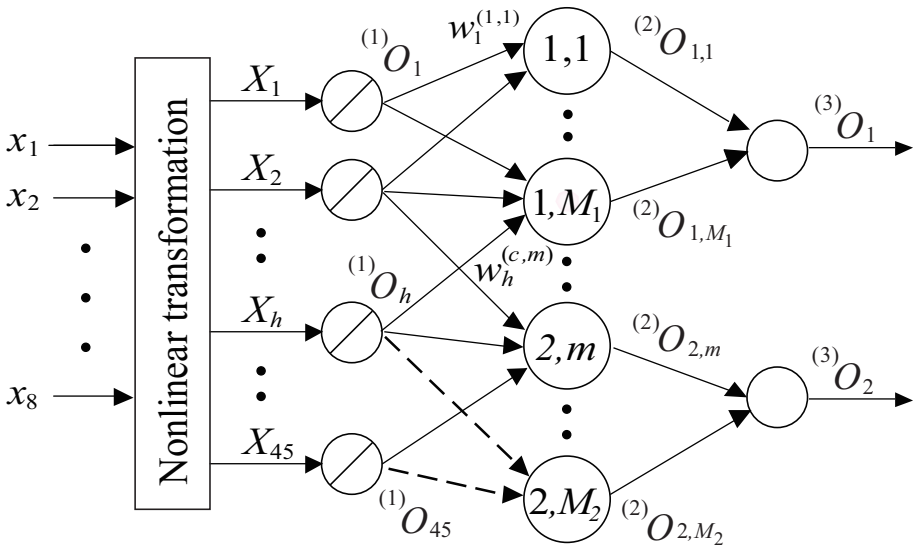

Fig. 3.2: Structure of the proposed log-linearized Gaussian mixture network

3.3 Experiments

The subjects were divided into two groups. One consisted of 15 patients with PD whose autonomic nervous function was abnormal (9 males and 6 females; mean age ± S.D.: 69.4 ± 8.5 yrs; Subjects A – O), and the other consisted of 10 patients with Parkinsonism whose autonomic nervous function was normal (4 males and 6 females; mean age ± S.D.: 73.7 ± 3.1 yrs; Subjects P – Y). Diagnostic outcomes in terms of whether the subjects' autonomic nervous function was normal were based on results of ^{123}-MIBG myocardial scintigraphy examination. Those with PD whose average gamma ray count (referred to as the H/M ratio) for both early and late images was between 1.10 and 1.99 were deemed to have abnormal autonomic nervous function, and those with Pism whose H/M ratios for both images were between 2.00 and 3.30 were deemed to have normal autonomic nervous function. Subjects suffering from Pism with multiple system atrophy (MSA) were removed from the analysis pool in this study because MSA can be identified via magnetic resonance imaging (MRI) of the head [43]. Informed

consent was obtained from all study subjects before the experiments were performed based on approval from the Ethics Committee of the National Hospital Organization Toneyama Hospital (clinical study number: 1015).

3.3.1 Diagnosis of Parkinson's Disease and Parkinsonism

To investigate accuracy and evaluation capability for PD/Pism diagnosis, the performance of the proposed system was experimentally verified. The average feature value for subjects in the PD group was compared with that of the proposed indices for the other group, and the diagnostic accuracy of the analysis results based on the proposed method was evaluated using receiver operating characteristic (ROC) analysis. The measurement data from five PD patients whose H/M ratios for both the early and late images were between 1.10 and 1.55. Results from five Pism patients whose H/M ratios for both the early and late images were between 2.00 and 3.00 were chosen as LLGMN learning data, and the other subjects' data were used as test data. The number of components for the LLGMN was set as 1, and Welch's t-test was used to compare values between PD and Pism. Differences were considered significant when p was smaller than 0.05.

3.3.2 Assessment of Phototherapy Effects

Phototherapy treatment involves bright light irradiation to stimulate dopamine production, suppress melanin production and improve circadian rhythm [41]. It is considered to have curative effects for non-motor symptoms of PD. Against such a background, the experiment described here was performed to verify phototherapy effects in treatment using the proposed method. Four PD patients (mean age ± S.D.: 70.3 ± 8.6 yrs) receiving phototherapy underwent HUT before and after the treatment. The learning data specified in 3.3.1 were used for this evaluation.

3.4 Results

Figures 3.3 (a) and (b) show examples of measured and analysis waves for the bed slopes, SBPs, DBPs, PPGs, and the stiffness parameter β for all measurement times from Sub. A with PD and Sub. P with Pism, respectively. The shaded area represents the period during which the table was tilted. The results indicate that the measured PPG amplitudes decreased and the measured stiffness parameter β increased with greater angles of tilt, and that PPG amplitudes increased and the measured stiffness parameter β decreased with smaller angles of tilt. Here, PPG amplitude progressively increased soon after the subject left the standing position. First, the stiffness parameter β of Sub. A temporarily increased soon after the standing position was left. Next, *beta* stabilized after progressively decreasing.

Figure 3.4 shows the extracted feature values x_1 to x_8. No significant differences were observed between the patients with PD and those with Pism for any of the feature values ((a): $p = 0.78$; (b): $p = 0.91$; (c): $p = 0.91$; (d): $p = 0.75$; (e): $p = 0.64$; (f): $p = 0.92$; (g): $p = 0.98$; (h): $p = 0.96$). In addition, the area under the curve (AUC) from the ROC analysis for the learning data described in Chapter 3.3.1 was calculated with each feature value to verify diagnostic accuracy. The results showed that individual single feature values cannot be used to accurately differentiate patients with and without abnormal autonomic nervous function. ((a): AUC = 0.56; (b): AUC = 0.56; (c): AUC = 0.64; (d): AUC = 0.52; (e): AUC = 0.52; (f): AUC = 0.52; (g): AUC = 0.60; (h): AUC = 0.56).

Figure 3.5 (a) compares results from autonomic nervous function abnormality markers between PD and Pism for all patients. The results indicate that autonomic nervous function abnormality markers differed significantly between patients with PD and those with Pism (autonomic nervous function abnormality marker for PD: $0.73 \pm$

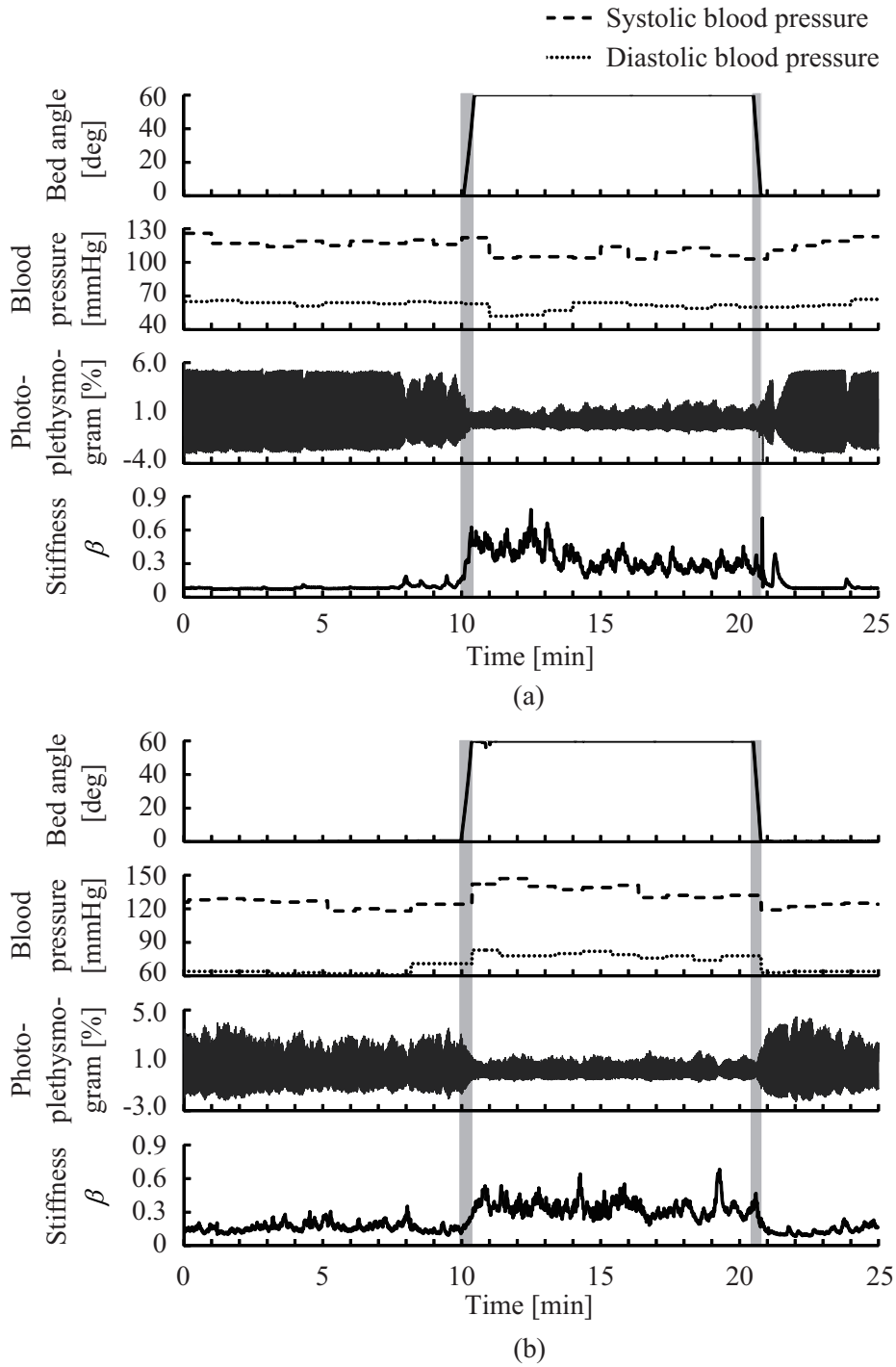

Fig. 3.3: Example of analysis waves: (a) Subject A (abnormal autonomic nervous function); (b) Subject P (normal autonomic nervous function)

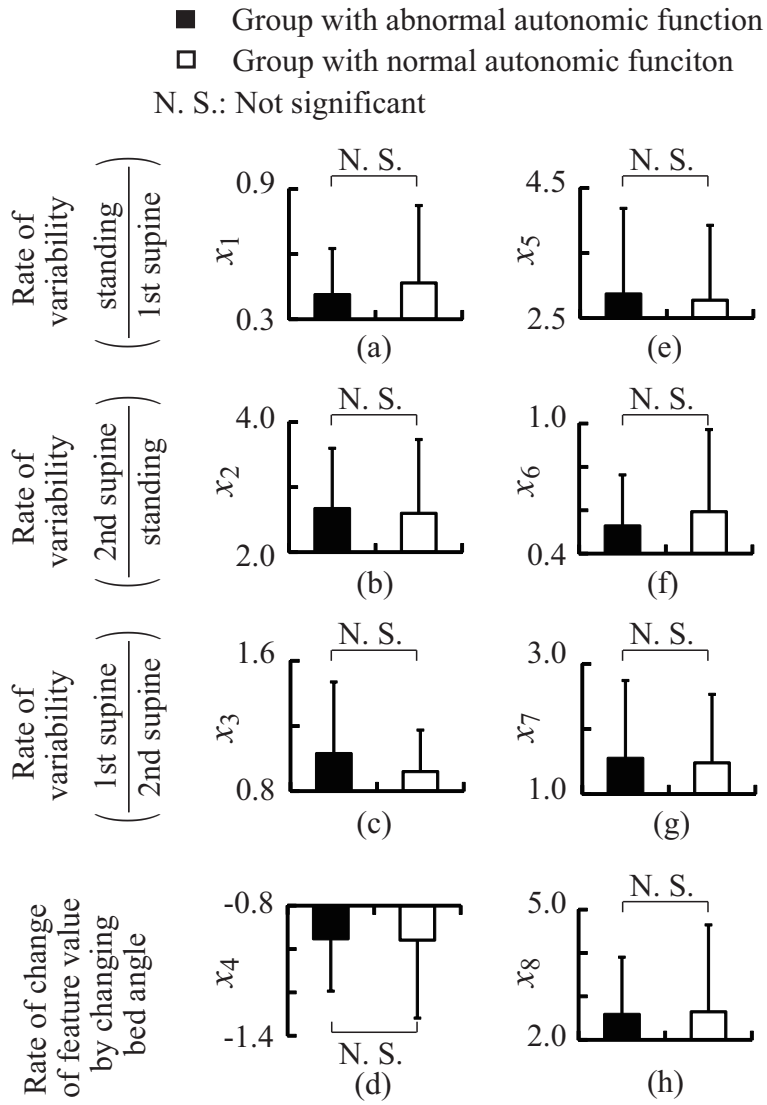

Fig. 3.4: Comparison of feature values between the abnormal autonomic nervous function group and the normal autonomic nervous function group: (a) x_1: rate of change in photoplethysmogram amplitude (standing position/first supine position); (b) x_2: rate of change in photoplethysmogram amplitude (second supine position/standing position); (c) x_3: rate of change in photoplethysmogram amplitude (second supine position/first supine position); (d) x_4: slope of regression line for photoplethysmogram amplitude as table tilts; (e) x_5: rate of change in stiffness parameter β (standing position/first supine position); (f) x_6: rate of change in stiffness parameter β (second supine position/standing position); (g) x_7: rate of change in stiffness parameter β (second supine position/first supine position); (h) x_8: slope of regression line for stiffness parameter β as table tilts

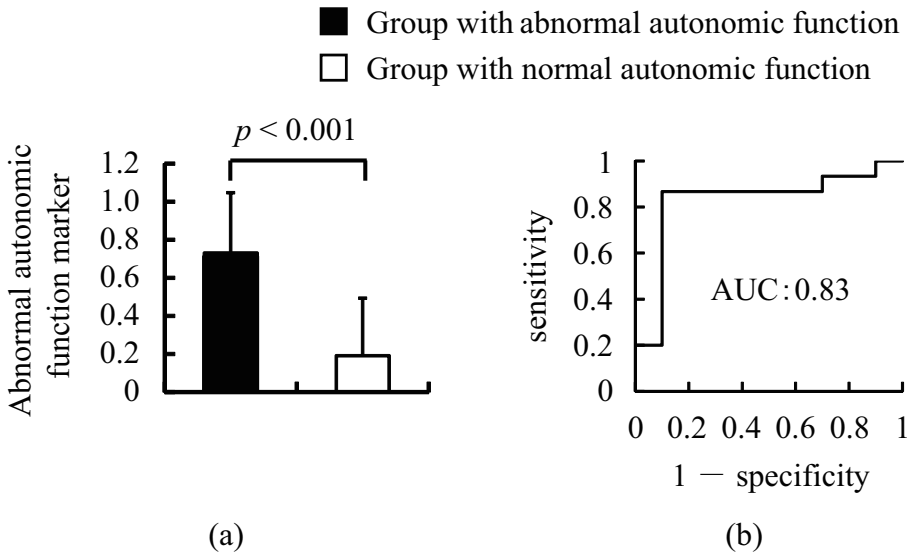

Fig. 3.5: Autonomic nervous function abnormality marker results: (a) comparison of autonomic nervous function abnormality markers between the abnormal autonomic nervous function group and the normal autonomic nervous function group; (b) ROC curve

Table 3.1: Analysis results: (a) learning data; (b) test data

(a) (%)

Abnormal identification by LLGMN	Autonomic function	
	abnormal	normal
Positive	100	0
Negative	0	100

(b) (%)

Abnormal identification by LLGMN	Autonomic function	
	abnormal	normal
Positive	80	20
Negative	20	80

0.32; for Pism: 0.19 ± 0.30, $p < 0.001$). Figure 3.5 (a) shows the results of ROC analysis involving the use of abnormal automatic nervous function markers. The AUC of the ROC curve from all subjects was 0.83.

Table 3.1 shows the diagnostic results obtained with the proposed method. The results showed that the sensitivity and specificity of both sets of patients (i.e., those with abnormal and normal autonomic nervous function) as determined using learning

Table 3.2: Changes in autonomic nervous function abnormality marker values before and after phototherapy

Subject	Positive probability of abnormal autonomic function		
	Before phototherapy	After phototherapy	Before phototherapy / After phototherapy
Sub. C	6.03×10^{-1}	4.14×10^{-1}	6.85×10^{-1}
Sub. D	8.39×10^{-1}	1.26×10^{-5}	1.50×10^{-5}
Sub. E	8.22×10^{-1}	7.45×10^{-1}	9.06×10^{-1}
Sub. K	9.27×10^{-1}	9.99×10^{-1}	1.08
Average	0.797 ± 0.137	0.539 ± 0.432	0.668 ± 0.473

data were 100%. Meanwhile, the sensitivity and specificity of both groups based on test data were 80%. The results of ROC analysis showed that the value of AUC calculated from learning data was 1, while that from test data was 0.76.

Table 3.2 shows autonomic nervous function abnormality marker values before and after phototherapy. The results showed that autonomic nervous function abnormality markers after phototherapy were lower than those before except for Sub. K (average marker before phototherapy: 0.798 ± 0.137; after: 0.539 ± 0.432). Two of four patients whose autonomic nervous function markers showed abnormality were diagnosed as having normal autonomic nervous function after phototherapy based on these markers.

3.5 Discussion

Section 3.4 shows the results of an experiment conducted to verify the proposed method's efficacy for diagnosis relating to autonomic nervous function. Figure 3.3 indicates a reduction in the measured PPG amplitude and an increase in the estimated stiffness parameter β with higher tilt table angles. A normal person's blood pressure

will not fall dramatically when a standing state is assumed because peripheral blood vessels narrow in order to maintain systemic circulation. It is assumed that vasoconstriction causes vascular volume decrease and artery induration, causing reduced PPG amplitude and an increase in the stiffness parameter β.

Figure 3.4 and the results of ROC analysis show no significant differences between the two patient groups for any of the independent indices, and diagnostic accuracy based on them was not superior. However, the variability of calculated average values differs between patients with and without abnormal autonomic nervous function for the variation coefficient of each index in Fig. 3.4. This is because the averages of one patient group may have been concentrated around a certain value, while those of the other were not. As a result, there were no significant differences in any feature values between the two groups, and the AUC of the ROC curve was also low. Accordingly, patient groups here are defined using a combination of all feature values based on the LLGMN [42] rather than being based on single feature values or on consideration of the cohesion or variability of feature values.

Figure 3.5 indicates that there was a significant difference in automatic function abnormality markers between the two patient groups, and that the AUC of the ROC curve for all subjects exhibited high accuracy (AUC: 0.827). Additionally, Table 3.1 indicates that the identification rate for learning data was 100%, which is very high with a combination of all feature values, and that the indication rate for test data was 80%, which is also relatively high. The results also show that the AUC of ROC analysis using the proposed method with learning data was 1, while that obtained using test data was 0.76. These values are higher than the 0.52 – 0.64 range obtained with individual feature values. As a result, it can be concluded that the proposed method enables successful evaluation of autonomic nervous function for patients with PD and

Pism. This study involved the use of learning data from 10 patients and test data from 15 patients. However, it may be challenging to obtain the same above number ratio of learning and test data in practical application. Here, the priority for diagnostic accuracy using the LLGMN is not the same number ratio of learning and test data but whether the LLGMN accurately learns general features of PD and Pism from learning data. There is a need to maximize the amount of learning data available (e.g., by adding test data) and to achieve greater accuracy in identification toward practical application.

As MIBG myocardial scintigraphy examinations are associated with the potential for radiation exposure, they cannot be performed repeatedly on the same patient due to the significant burden involved. Against such a background, the proposed method is intended to enable quantitative assessment for the effects of performing phototherapy instead of MIBG myocardial scintigraphy. The results shown in Table 3.2 indicate that at least two out of four patients exhibited improved autonomic nervous function after phototherapy based on consideration of autonomic nervous function abnormality markers. Accordingly, it can be concluded that the method supports quantitative evaluation for phototherapy. However, more data are needed to allow examination of the method in practical use.

3.6 Concluding Remarks

This Chapter proposes a new method to support the diagnosis of PD, which is associated with abnormal autonomic function. As PD and Pism have similar symptoms but different treatment methods, accurate diagnosis is required. The proposed method can be applied to identify both diseases based on the abstraction of changes in arterial viscoelastic properties and digital pulse volume determined using HUT (a postural

change test) as a feature value, and on the judgment of normal/abnormal autonomic nervous function using a probabilistic neural network. The two conditions cannot not be differentiated on the basis of individual feature values alone, but autonomic function was precisely evaluated with the proposed method. The conditions were differentiated based on learning with an NN combination of all indicators rather than individual feature values. In addition, the feasibility of quantitative evaluation to determine the effects of light therapy using the proposed method for patients undergoing autonomic function treatment was demonstrated even in cases without ^{123}I-MIBG myocardial scintigraphy testing.

Chapter 4

Objective Assessment of Pain During Electrocutaneous Stimulation Based on a Peripheral Arterial Viscoelastic Index

4.1 Introduction

Pain intensity is associated with sympathetic nerve activity, which in turn is related to the characteristics of peripheral arterial dynamics. These relationships offer potential for the monitoring of analgesic effects during surgical operations and treatment based on real-time measurement of changes in the characteristics of arterial dynamics related to sympathetic nerve activity. This chapter proposes a novel technique for the objective assessment of pain intensity based on changes in peripheral arterial stiffness β that result from peripheral sympathetic nerve activity. Stiffness β is calculated from continuous arterial pressure and photoplethysmograms on a beat-by-beat basis using a log-linearized peripheral arterial model that incorporates consideration of the nonlinear relationship between photoplethysmograms and arterial pressure. The chapter also discusses order effects associated with electrostimulation and describes the results of analysis performed to elucidate the relationships between electrostimulation and

pain/subjective pain intensity, between subjective pain intensity and changes in the stiffness parameter β, and between changes in this parameter and electrostimulation causing pain.

4.2 Quantification of Sympathetic Nerve Activity

4.2.1 Relationship Between Pain and Sympathetic Nerve Activity

There is a strong connection between pain and sympathetic nerve activity [1]. Stimulus information is transformed into bioelectric signals through nociceptors when noxious stimuli are applied. These signals are propagated to the cerebral cortex via the spinal cord, medulla oblongata, and thalamus, causing the person to perceive pain. At the same time, the sympathetic nervous system is activated by the propagated bioelectric signals, and this causes blood vessels to constrict [1]. Clarification of the relationship between pain sensation and sympathetic nerve activity thus makes it possible to objectively assess pain intensity by measuring sympathetic nerve activity.

4.2.2 Estimation Method for Sympathetic Nerve Activity

Sakane *et al.* modeled the dynamic characteristics of the peripheral arterial wall using a linear mechanical arterial impedance model based on measured photoplethysmograms (PPGs) and blood-pressure variations. The same authors also proposed a method for estimating peripheral sympathetic nerve activity using the arterial impedance model [23]. Additionally, Kohno *et al.* estimated pain intensity using the arterial impedance model and analyzed the relationship between pain intensity and the dynamic characteristics of the peripheral arterial wall [44]. However, non-linear characteristics of arterial stiffness were not taken into consideration in the arterial impedance model used by Kohno *et al.* for the estimation of pain intensity, and as a result, evalu-

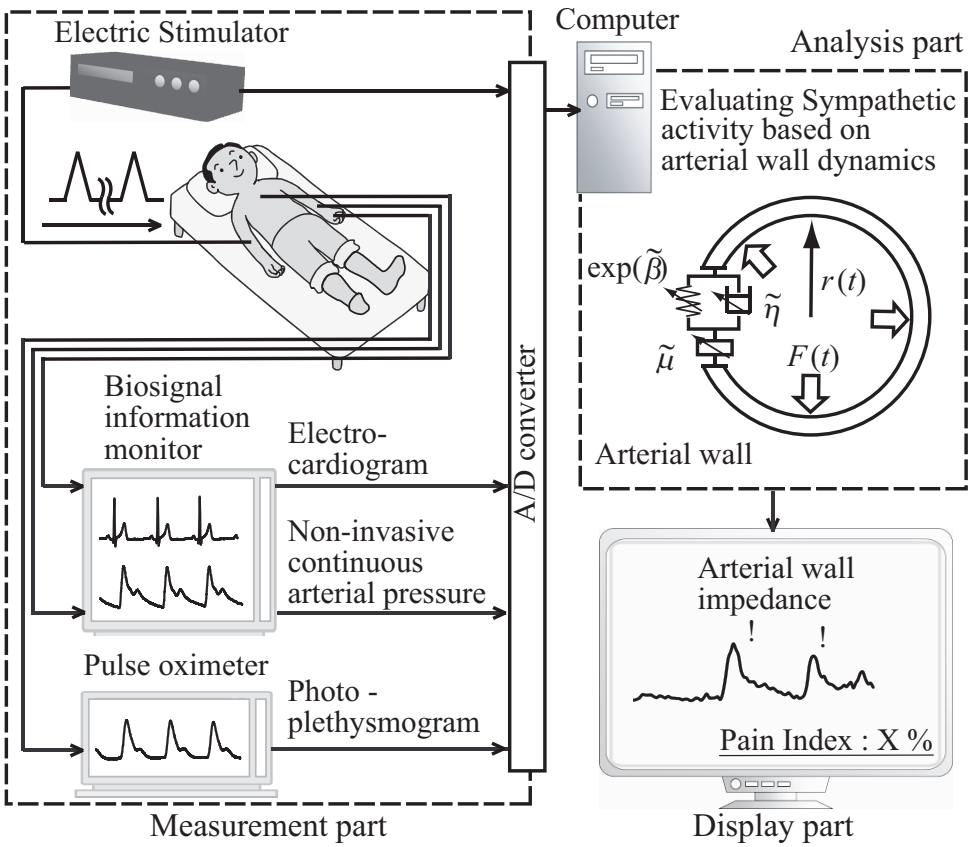

Fig. 4.1: Overview of the proposed system

ation indices of pain intensity based on arterial impedance depended on blood-pressure variations that did not relate to pain intensity. This chapter presents a novel quantitative method for evaluating pain intensity using the log-linearized peripheral arterial viscoelastic model.

Figure 4.1 shows the proposed system for evaluating sympathetic nerve activity in response to transcutaneous electrostimulation. The system consists of three units: the measurement unit, which simultaneously measures coincident biological signals and the transcutaneous electrical stimulation applied to subjects; the analysis unit, which calculates indices of sympathetic nerve activity from measured biological signals using the log-linearized peripheral arterial model; and the evaluation unit, which evaluates

Fig. 4.2: Electrocutaneous stimulation site

sympathetic nerve activity using the calculated indices.

In the measurement unit, biological signals and transcutaneous electrical stimulation signals are measured simultaneously. Electrical stimulation signals $I(t)$, which are triangular pulse currents, are applied to the skin surface on the inner part of the right forearm (Figure 4.2). The system measures electrocardiogram values, noninvasive continuous blood pressure, and PPGs as biological signals when electrical stimulation is applied. Electrocardiogram values are measured with a three-lead electrocardiograph, non-invasive continuous blood pressure $P_b(t)$ is measured at the left radial artery, and photoplethysmograms $P_l(t)$ are measured on the left index finger. The maximum amplitude of the electrical stimulation signals I_{max} and all measured biological signals are saved on a computer using an analog/digital converter.

In the analysis unit, sympathetic nerve activity is estimated as electrical stimulation is applied. With every heartbeat, the indices of sympathetic nerve activity are calculated from the dynamic characteristics of the peripheral arterial wall using the log-linearized peripheral arterial viscoelastic model.

$$\begin{aligned} F(t) &= \tilde{\mu}\ddot{r}(t) + \tilde{\eta}\dot{r}(t) \\ &\quad + \exp\{\tilde{\beta}dr(t) + F_{\tilde{\beta}_0} + F_{\tilde{\beta}_{nl}}(r(t))\} \end{aligned} \tag{4.1}$$

Here $\tilde{\mu}$, $\tilde{\eta}$, and $\tilde{\beta}$ are the arterial wall's inertia, viscosity, and stiffness, respectively. $F(t)$, $r(t)$, $dr(t)$, $\dot{r}(t)$, and $\ddot{r}(t)$ represent normal force in the direction of the arterial wall, the arterial diameter, the displacement of the arterial diameter, the velocity of the arterial diameter, and the acceleration of the arterial diameter, respectively all measured at the arbitrary time t. $F_{\tilde{\beta}_0}$ is the standard blood pressure and $F_{\tilde{\beta}_{nl}}$ is a force originating in the vein. It is assumed that the blood pressure $P_b(t)$ is equal to the force $F(t)$ per unit area, and there is a proportionate relationship between the displacement of the arterial diameter and the PPG (see Appendix A). Accordingly, the Equation (4.1) can be expressed as follows:

$$\begin{aligned} P_b(t) &= \mu\ddot{P}_l(t) + \eta\dot{P}_l(t) \\ &\quad + \exp\{\beta P_l(t) + P_{b\beta_0} + P_{b\beta_{nl}}(P_l(t))\} \end{aligned} \tag{4.2}$$

Here $P_b(t)$, $P_l(t)$, $\dot{P}_l(t)$, and $\ddot{P}_l(t)$ are the blood pressure, the arterial diameter, the velocity of the arterial diameter, and the acceleration of the arterial diameter, respectively all measured at the arbitrary time t. $P_{b\beta_0}$ is the standard blood pressure and $P_{b\beta_{nl}}$ is a force originating in the vein. μ, η, and β are calculated for each heartbeat from the Equation (4.2) using the least-squares method. As it has been reported that arterial stiffness β prominently responds to direct sympathetic nerve stimuli, the authors used arterial stiffness β as an evaluation index to estimate changes in sympathetic nerve activity during transcutaneous electrical stimulation accompanied by pain. However, R^2 (the coefficient of determination between the measured blood-pressure values $P_b(t)$ and the estimated blood-pressure values) is calculated. Here the estimated blood-pressure values were calculated from the estimated arterial impedance parameters μ, η, and β, as well as from the measured photoplethysmograms $P_l(t)$. The use of an approximate quantity for the estimated stiffness parameter β is justified if the value of the coefficient of determination is 0.9 or more because this enables exclusion of results associated with

unexpected artifacts such as bodily motion.

Finally, the evaluation part evaluates and displays the relationship between the applied electrical stimulus and the arterial stiffness parameter β. In this study, the proposed system was used to evaluate sympathetic nerve activity during applied transcutaneous electrical stimulation.

4.3 Electrical Stimulation Experiments

To verify the ability of the proposed system to objectively evaluate pain intensity produced by transcutaneous electrical stimulation, electric stimulation experiments were performed on healthy subjects in a wakeful state using the system. The system measured changes in the arterial stiffness parameter β and in pain as measured on the numeric rating scale when the amplitude of the stimulus current was changed. The subjects participated in the experiment in a wakeful state so that they could subjectively assess pain caused by transcutaneous electrical stimulation.

Incidentally, it is known that psychological stress, including fear and tension, causes sympathetic nerve activity [45]. Consequently, such activity may be triggered by psychological stress or fear caused by electrical stimulation associated with pain when the stimulation is applied to subjects in a wakeful state. The psychological stress caused by the stimulus might be controllable by the application of multiple stimuli. However, for the purposes of liability avoidance, it was decided to apply the stimulus to each subject only once. First, the test protocol that enables control of psychological stress associated with the electrical stimulus was verified as valid. Next, the relationships among the load current, the value on the numeric rating scale, and the arterial stiffness parameter β were experimentally evaluated according to the above test protocol.

Each subject was in a supine position, and the system in Figure 4.1 was used for the experiment. The stimulating current, which was a triangular pulse current with

a pulse width of 0.3 ms at 50 Hz, was produced by an electrical stimulator (SEN-3041, Nihon Kohden Corp., Tokyo, Japan), an isolator (SS-203J, Nihon Kohden Corp., Tokyo, Japan), and a function generator (FG120, Yokogawa Electric Corp., Tokyo, Japan). While the stimulating current was being applied to the subject, electrocardiogram signals and non-invasive left radial arterial blood pressure were measured using a biological information monitor (BP-608 Evolution II CS, Omron Colin, Tokyo, Japan). PPGs were measured using a pulse oxymeter (OLV-3100, Nihon Kohden Corp., Tokyo, Japan). Data on these biological signals and the stimulating current were stored at 1,000 Hz on a computer using an analog/digital converter (CSI-360116, Interface Corp., Hiroshima, Japan). To relieve subjects of as much psychological stress as possible, the maximum current amplitude of the transcutaneous electrical stimulation was changed by 1.5 mA every 30 seconds, which is not a random current variation. The response of the stiffness parameter β to the stimulus was evaluated based on the maximum β value during a 30-second contact stimulus kept at maximum current amplitude I_{max}. Humans have a function called adaptability and another called the negative feedback mechanism [1, 46]. Adaptability is the body's ability to gradually reduce upward afferent impulses during prolonged stimuli [1], and the negative feedback mechanism inhibits sympathetic nerve activity and lowers blood pressure when blood-pressure elevation causes an increase in the excitatory input of an arterial baroreceptor [46]. In this study, the maximum stiffness parameter β was adopted as an evaluation index to eliminate the influences of adaptability and the negative feedback mechanism as much as possible. Immediately after each shift in the stimulating current, the subjects reported the subjective pain level vocally and evaluated it using the numeric rating scale [28–30], which ranks pain levels in 11 increments from 0 to 10 (no pain being 0 and maximum pain being 10).

In accordance with the Declaration of Helsinki, informed consent was obtained from all study subjects before the experiments were performed, and the approval of the Hiroshima University Ethics Committee was also obtained. The safety of the electrical stimulator used in this study was verified in accordance with IEC 60601. To ensure the subjects' safety and limit their physical burden, strong stimuli (those above seven on the numeric rating scale) were not applied.

4.3.1 Experimental Trials for Electrocutaneous Stimulation Task

The purpose of the first test was to establish a task protocol that could be used in the second test to control subjects' psychological stress. Six healthy male subjects (A – F; mean age ± S.D.: 22.2 ± 0.9 yrs) were chosen for the experiment. The test included two tasks: a valley-type stimulation task, in which the stimulating current was 9 mA at the beginning, then was gradually reduced to 0 mA, and then was gradually increased again to 9 mA; and a mountain-type stimulation task, in which the stimulating current was 0 mA at the beginning, then was gradually increased to 9 mA, and then was gradually reduced again to 0 mA.

To determine the effects of the psychological stress of each task on the stiffness parameter β, the value of this parameter for stimulus 0 mA (not intended to produce pain) and stimulus 9 mA (intended to produce pain) were compared in each task. Bonferroni correction was used to determine the significance of differences in the stiffness parameter β (a necessary step for avoiding multiplicity issues). Differences were considered significant when results showed $p < 0.0167$.

4.3.2 Pain-level Evaluation Test

The capacity for objective pain assessment using the stiffness parameter β in the

proposed system was experimentally verified. Thirteen healthy male subjects (A – M; mean age ± S.D.: 22.7 ± 1.1 yrs), including the same individuals specified in Chapter 3.1, were chosen for the experiment. The experimental protocol was based on the task (detailed in 4.3.1) verified as having the ability to reduce psychological stress. To evaluate changes caused in the stiffness parameter β by the stimulus, the stiffness parameter β was normalized based on the measured maximum value of β at non-stimulation (I_{max} was 0 mA). Here the normalized stiffness parameter is defined as β_{n}. To verify the relationship between subjective pain evaluation and the stiffness parameter β associated with pain, averages and standard deviations of the normalized stiffness parameter β_{n} and the value on the numeric rating scale for each stimulating current I_{max} were calculated for all subjects. The coefficients of correlation and the approximate curve between I_{max} and the value on the numeric rating scale between I_{max} and β_{n} and between β_{n} and the value on the numeric rating scale were also calculated.

4.4 Results

4.4.1 Experimental Trials for Electrocutaneous Stimulation Task

Figure 4.3 shows the measured signals from Subject A during the application of the valley-type stimulus. These are the maximum current amplitude of transcutaneous electrical stimulation I_{max}, non-invasive blood-pressure $P_b(t)$, and photoplethysmograms $P_l(t)$, respectively. Figure 4.3 indicates that blood pressure increased when the current amplitude I_{max} was high, and that the peak-to-peak amplitude PPG measured from beat to beat (called the PPG amplitude [21]) decreased with the high-stimulation current. Highly significant correlations were observed between the current amplitude I_{max} and the maximum blood-pressure value in each 30-second interval P_{bmax} and between the current amplitude I_{max} and the maximum PPG in each 30-second interval

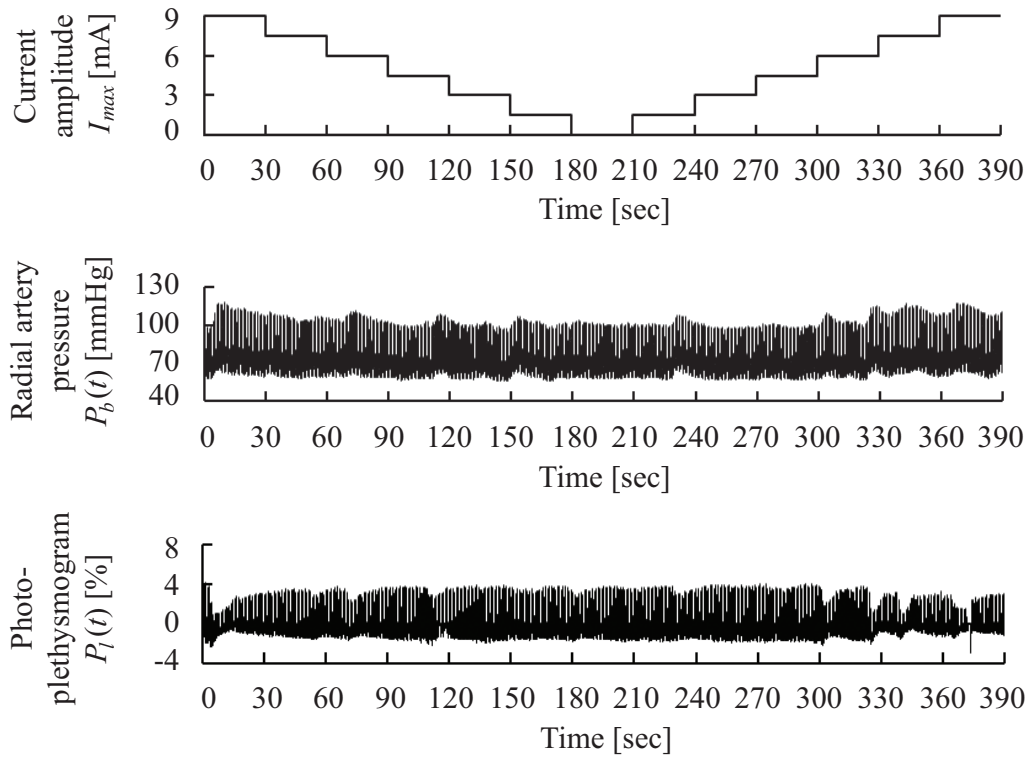

Fig. 4.3: Measured radial arterial pressures and photoplethysmo grams from Subject A when the valley-type electrocutaneous stimuli were applied

$P_{lmax}(t)$: respectively, I_{max} vs. $P_{bmax}(t)$: $R = 0.80$ ($p < 0.01$), I_{max} vs. $P_{lmax}(t)$: $R = -0.77$ ($p < 0.01$).

Figure 4.4 shows the analysis results for Subject A. Figure 4.4 (a) shows the analysis results from the mountain-type task and (b) those from the valley type. From top to bottom, each figure shows the maximum current amplitude I_{max}, the stiffness parameter β, and the values on the numeric rating scale. The results indicate that the changes in the magnitude of the electrical current caused differences in the stiffness parameter β. Here it is assumed that the cause of changes in the stiffness parameter β is psychological stress when the stiffness parameter β changes in the absence of stimulus. The stiffness parameter β when I_{max} equaled 0 mA was compared with that when I_{max}

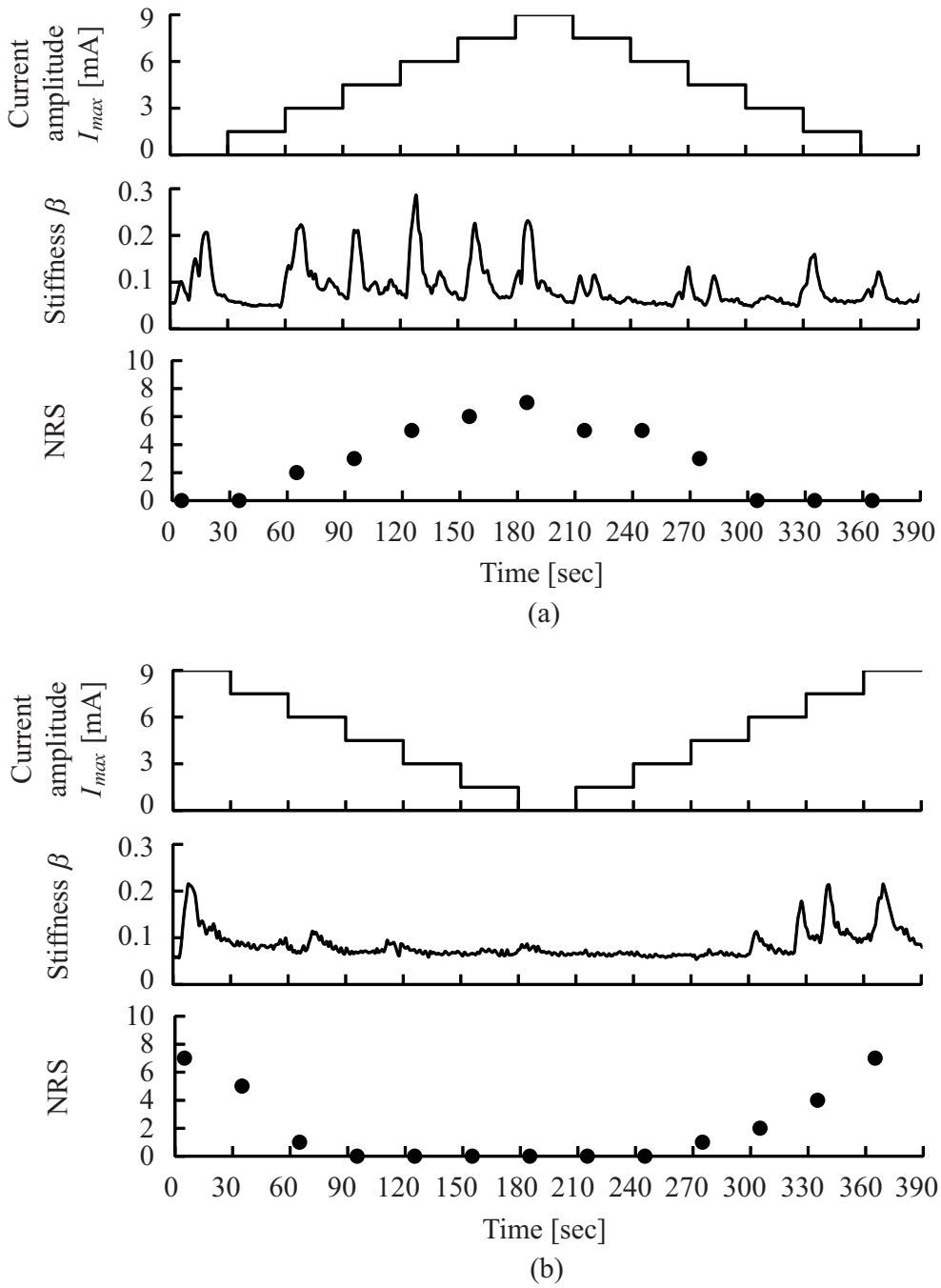

Fig. 4.4: Estimated results of stiffness parameter β and recorded self-reporting NRS values during electrocutaneous stimulation (Subject A): (a) the hill-type stimuli, (b) the valley-type stimuli

equaled 9 mA in order to determine the influence of psychological stress on the stiffness parameter β. Figure 4.5 (a) shows the analysis results of the mountain-type task and (b) those of the valley-type task. Both sets of results were obtained with all subjects. Figure 4.5 (a) shows that the stiffness parameter β significantly differed according to whether the stimulation current I_{max} was 9 mA for 180 – 210 seconds or 0 mA for 360 – 390 seconds ($p < 0.05$). Meanwhile, the results in Figure 4.5 (b) indicate that the stiffness parameter β significantly differed according to whether the stimulation current I_{max} was 9 mA for 0 – 30 seconds or 0 mA for 180 – 210 seconds, and whether it was 0 mA for 180 – 210 seconds or 9 mA for 360 – 390 seconds ($p < 0.05$).

4.4.2 Pain-level Evaluation Test

Figure 4.6 shows a set of results from a valley-type task that were chosen from among the results of the experimental trials conducted for transcutaneous electrical-stimulation task selection. From top to bottom, the figure shows the relationship between I_{max} and β_n, that between I_{max} and the values on the numeric rating scale, and that between β_n and the values on the numeric rating scale. The mean values were calculated from data on all subjects. Figure 4.6 indicates that the normalized stiffness parameter β_{n} significantly increased along with increases in I_{max} ($R^2 = 0.77$ ($p < 0.05$)). The value on the numeric rating scale also significantly increased along with increases in I_{max} or in the normalized stiffness parameter β_{n}. As the numeric rating scale is restricted to a range of 0 to 10, the relationships between the value on this scale and I_{max} and that between the value on the scale and the normalized stiffness parameter β_{n} were approximated using a sigmoid function, and were modeled with high correlations: respectively, I_{max} vs. NRS: $R^2 = 0.91$ ($p < 0.01$), β_{n} vs. NRS: $R^2 = 0.92$ ($p < 0.01$).

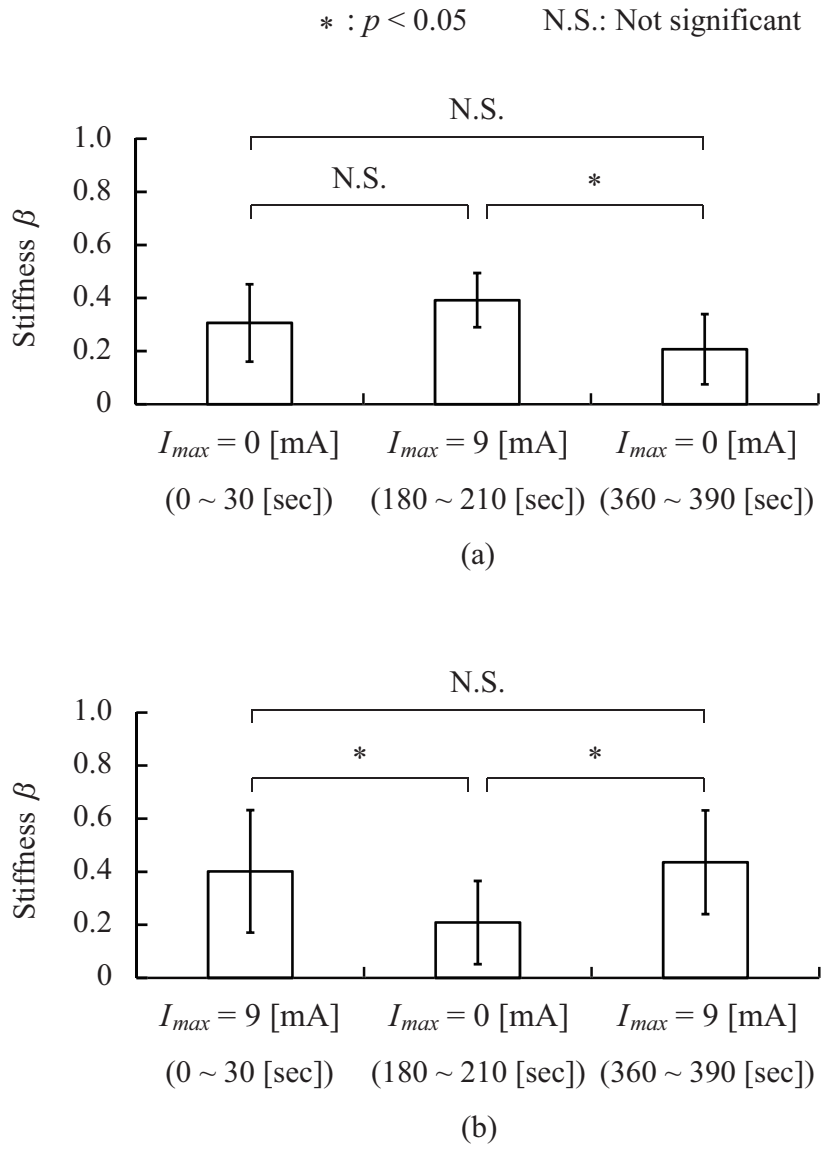

Fig. 4.5: Comparison of stiffness β among the period from 0 second to 30 seconds, from 180 seconds to 210 seconds, and from 360 seconds to 390 seconds: (a) the hill-type electrocutaneous stimuli were applied. 9 mA of electrical stimulus was applied during the period from 180 seconds to 210 seconds and 0 mA of electrical stimulus was applied during the period from 0 second to 30 seconds and from 360 seconds to 390 seconds, (b) the valley-type electrocutaneous stimuli were applied. 9 mA of electrical stimulus was applied during the period from 0 second to 30 seconds and from 360 seconds to 390 seconds and 0 mA of electrical stimulus was applied during the period from 180 seconds to 210 seconds

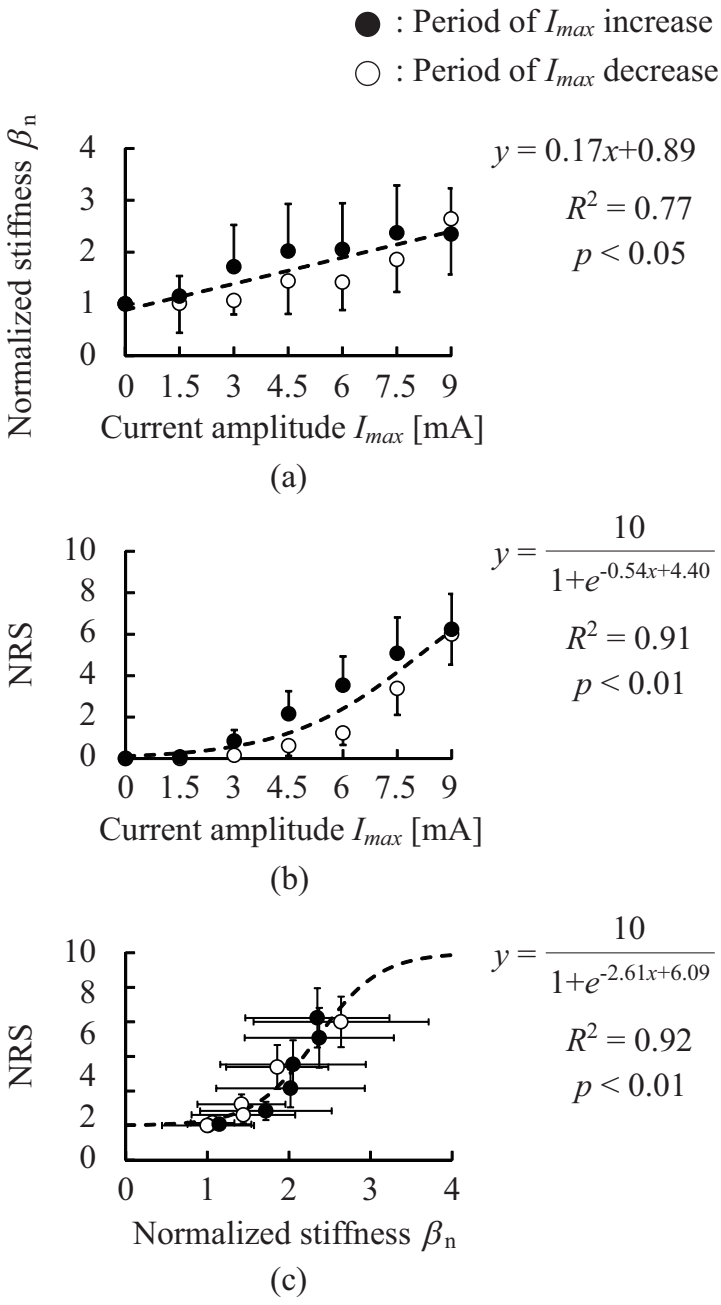

Fig. 4.6: Relationships between the applied valley-type electrocutaneous stimulus intensity and the indices for evaluating the pain intensity: (a) relationship between estimated normalized stiffness β_{n} and the applied current stimulus intensity I_{max}, (b) relationship between self-reported NRS values and the applied current stimulus intensity I_{max}, (c) relationship between self-reported NRS values and estimated normalized stiffness β_{n}

4.5 Discussion

Figure 4.3 shows that the PPG amplitude changed with the magnitude of the maximum current amplitude I_{max}. Previous research has shown that fluctuation in the PPG amplitude presents with an activated state of the sympathetic nervous system [21]. Accordingly, changes in PPGs potentially indicate changes in sympathetic nerve activity. Correspondingly, the changes in I_{max} in Figure 4.3 caused variability in blood pressure as well as in PPGs. Evaluation of sympathetic nerve activity therefore requires consideration of variability in both PPGs and blood pressure.

Figure 4.4 shows that the stiffness parameter β changed when the stimulation current was applied to the subjects' skin in both the mountain-type task and the valley-type task. Arterial stiffness depends on sympathetic nerve activity [47]. As these functions cannot be voluntarily controlled, the sympathetic nerve responded to transcutaneous electrical stimulation. However, Figure 4.4 (a) shows that the stiffness parameter β responded during a 30-second interval (right after the beginning of the task) that was a non-stimulation period. This was because sympathetic hyperactivity had been activated; that is, the subjects felt psychological stress as a result of the transcutaneous electrical stimulation. The stiffness parameter β responded dramatically during increases in the stimulating current, just as it had before the first stimulation. However, the responses of the stiffness parameter β during decreases in the stimulating current differed significantly from those observed during increases. These results show that the subjects experienced psychological stress and sympathetic hyperactivity. This occurred because they were unable to viscerally imagine the maximum stimulus of the mountain-type task until they felt it for themselves. Meanwhile, the stiffness parameter β responded dramatically to an initial stimulus, and the stiffness parameter β of the valley-type task showed a response during increases and decreases of the stimulat-

ing current that was similar to that of the mountain-type task during corresponding increases and decreases. Subjects also felt psychological stress in the valley-type task. However, they were able to perceive the strongest stimulating current at the beginning of the stimulation, and this is considered to have reduced the psychological fear that resulted from subsequent increases in the stimulating current.

As shown in Figure 4.5 (a), in the mountain-type task the stiffness parameter β responded similarly both to the application of the strongest stimulating current (I_{max} was 9 mA for 180 – 210 seconds) and to non-stimulation (I_{max} was 0 mA for 0 – 30 seconds). The major reason for this was that the psychological stress felt during non-stimulation was as great as that experienced when the strongest stimulating current was applied. As shown in Figure 4.5 (b), in the valley-type task the stiffness parameter β when the strongest stimulating current (I_{max} was 9 mA for 0 – 30 seconds and 360 – 390 seconds) was applied differed significantly from the same parameter during periods of non-stimulation (I_{max} was 0 mA for 180 – 210 seconds). This shows that the effect of psychological fear on the stiffness parameter β was removed by this task.

The result in Figure 4.6 (a) indicates that increased stimulating current led to a significant increase in the normalized stiffness parameter β_{n}. As the valley-type task keeps the effects of psychological fear under control, it is likely that involuntary sympathetic hyperactivity associated with extraneous stimuli [1] gave rise to the response of the normalized stiffness parameter β_{n}. As shown in Figure 4.6 (c), the relationship between subjective pain intensity (measured using the numeric rating scale) and the calculated normalized stiffness parameter β_{n} can be expressed approximately using a sigmoid function [48] similar to that representing the input-output characteristics of nerve cells. The sigmoid function was limited to a range of 0 to 10 in accord with the range of the numeric rating scale. The results show that the estimated values on the

numeric rating scale calculated from the normalized stiffness parameter β_{n} and from approximate mathematical expressions may enable objective and quantitative evaluation of human pain intensity.

It can therefore be concluded that, in the valley-type electrical stimulus experiment, there were statistically significant relationships among the normalized stiffness parameter β_{n} (which is under the control of sympathetic nerve activity), the stimulating current I_{max}, and the values on the numeric rating scale. The normalized stiffness parameter potentially enables objective assessment of levels of pain in cases where patients are unable to voluntarily express pain due to physical difficulty or anesthesia.

4.6 Concluding Remarks

This Chapter proposes a system for subjective and quantitative evaluation of human subjective pain intensity. Sympathetic activity associated with painful transcutaneous electrical stimulation was evaluated, and a statistically significant correlation among changes in arterial stiffness at peripheral points controlled by sympathetic nerve activity, transcutaneous electrical stimulation levels and subjective pain levels was observed. The relationship between normalized arterial stiffness β_n and transcutaneous electrical stimulation was successfully expressed by the sigmoid function, and the feasibility of objective pain evaluation based on measurement of normalized arterial stiffness βn was demonstrated.

Chapter 5

Conclusion

This dissertation proposes a novel peripheral arterial viscoelastic model that supports the monitoring of local autonomic function. To enable evaluation only of changes in the mechanical characteristics of an artery related to autonomic nerve activity, the proposed model allows (i) quantitative evaluation to identify the mechanical characteristics of the arterial wall based on impedance parameters such as stiffness, viscosity and inertia, (ii) estimation of stiffness factors considered unrelated to sympathetic nerve activity, such as the non-linear relationship between artery diameter and intra-arterial pressure, and (iii) elucidation of specific characteristics of peripheral arteries, such as arterial effects and arteriolar accumulation. An arterial characteristic index to support monitoring of autonomic nerve activity was then proposed based on the model. The method enables clarification of temporal changes in the proposed indicators, making it suitable for patient monitoring during endoscopic thoracic sympathectomy, differential examination between Parkinson's disease and Parkinsonism in the head-up tilt testing, and subjective/quantitative evaluation of pain.

Chapter 2 outlines an arterial mechanics model based on mechanical impedance in which intra-arterial pressure dependency specific to peripheral arteries is considered, and proposes a log-linearized peripheral arterial viscoelastic index that can be used to

clarify sympathetic activity. The validity and effectiveness of the proposed index were considered in two experiments. In the supine body roll test, the validity of the model and the related estimation method were demonstrated based on Lissajous curves of blood pressure vs. plethysmograms and the high correlation between estimated and actual blood pressure values. For changes in arm elevation during peripheral artery monitoring, the proposed indicator reduced the effects of intra-arterial pressure better than the conventional model according to comparison of changes in the stiffness $\tilde{K}$ of the conventional arterial mechanics model and the stiffness β of the proposed indicator. In endoscopic thoracic sympathectomy, stiffness β varied in response to surgical treatment, and acute sympathetic nerve activity was accurately determined. Further, immediately after the right sympathetic nerve was blocked, no reaction was observed in stiffness β monitored in the right sympathetic nerve during stimulation of the left sympathetic nerve, demonstrating that stiffness β can be used to evaluate local sympathetic nerve activity.

Chapter 3 proposes a new method to support the diagnosis of Parkinson's disease, which is associated with abnormal autonomic function. As Parkinson's disease and Parkinsonism have similar symptoms but different treatment methods, accurate diagnosis is required. The proposed method can be applied to identify both diseases based on the abstraction of changes in arterial viscoelastic properties and digital pulse volume determined using head-up tilt test (a postural change test) as a feature value, and on the judgment of normal/abnormal autonomic nervous function using a probabilistic neural network. The two conditions cannot not be differentiated on the basis of individual feature values alone, but autonomic function was precisely evaluated with the proposed method. The conditions were differentiated based on learning with an neural network combination of all indicators rather than individual feature values. In addi-

tion, the feasibility of quantitative evaluation to determine the effects of light therapy using the proposed method for patients undergoing autonomic function treatment was demonstrated even in cases without ^{123}I-MIBG myocardial scintigraphy testing.

Chapter 4 proposes a system for subjective and quantitative evaluation of human subjective pain intensity. Sympathetic activity associated with painful transcutaneous electrical stimulation was evaluated, and a statistically significant correlation among changes in arterial stiffness at peripheral points controlled by sympathetic nerve activity, transcutaneous electrical stimulation levels and subjective pain levels was observed. The relationship between normalized arterial stiffness β_{n} and transcutaneous electrical stimulation was successfully expressed by the sigmoid function, and the feasibility of objective pain evaluation based on measurement of normalized arterial stiffness βn was demonstrated.

Next, future tasks are discussed. First, stiffness β calculated using the log-linearized peripheral arterial viscoelastic model is not easily affected by blood pressure changes unrelated to sympathetic nerve activity. However, as the proposed method targets characteristics of arteries in vivo, genuine values of arterial characteristics are not evaluated. Accordingly, comparison based on arterial viscoelasticity involving excited arteries or phantom experiments with assumed human arteries is needed. Additionally, variations in the extent of change in stiffness β related to gender or age require further consideration. Nevertheless, autonomic nerve activity can be readily compared between subjects based on statistical data analysis.

Second, learning data were collected from five patients with Parkinson's disease and five patients with Parkinsonism in this study. The ratio of identification for these learning data was 100%, and a high rate of 80% was also observed among 15 patients for whom learning data were not collected. However, greater identification precision

is desired for practical application, and more learning data are therefore required. In future study, the number of subjects must be increased and the potential for further experimental verification and other methods should be considered. In addition, stiffness β was simply assumed in the proposed system due to the use of a generally accepted oscillometric automatic sphygmomanometer in the study. The use of a continuous sphygmomanometer will support the identification of variations in stiffness β and allow more accurate evaluation of autonomic nervous function. Accordingly, verification of the proposed method using a continuous sphygmomanometer is required.

Third, stiffness β assumed in the proposed method is an indicator for the evaluation of changes in arterial properties associated with exacerbation of the sympathetic nerve. It is useful in situations where the sympathetic nerve is exacerbated, such as those involving painful stimulation. However, objective evaluation of various factors relating to subjects themselves (such as the degree/type of pain experienced and mental anxiety associated with painful stimulation) was not performed, and the influence of these factors on stiffness β must be verified. Consequently, future studies should include consideration of brain activity evaluation based on fMRI during pain sensation, investigation of brain activation sites and degrees of activation, subjective pain, stimulation levels and individual bigamous relationships among transcutaneous electrical stimulation, brain activity evaluation based on fMRI, human subjective pain, and stiffness β. As brain function can be evaluated, the question of whether stiffness β reactions are caused by actual pain or by psychological factors such as phantom pain can be discussed. In this way, automatic nerve activation levels can be more accurately evaluated subjectively and quantitatively. Additionally, changes associated with surgical events depending on the dose of anesthetic can be monitored using the proposed method even under full anesthesia. The proposed method may thus also support the

detection of anesthetic over-administration or under-administration. Administration of anesthesia at levels that do not result in significant stiffness β changes during surgery is expected to support the maintenance of anesthetic effects, early recovery.

Finally, the potential of a log-linearized peripheral arterial viscoelastic index is discussed. The proposed indicator is considered useful in the evaluation of human conditions in various situations. By way of example, changes in stiffness β after a period of minutes or hours can be predicted mechanically using this indicator, and this can be applied in risk prediction for ICU patients. Additionally, both autonomic nerve activity and the steady state of an artery can be predicted based on a combination of stiffness β and viscosity η, and this can be used to support diagnosis of arteriosclerosis. Further, the development of a system that incorporates intuitive feedback of the pain felt by a patient to a therapist will support more effective rehabilitation. The ability to evaluate changes in mental condition using the proposed indicator will also allow quantitative evaluation of stress tolerance, depression, sleep quality and other considerations. A portable sphygmomanometer or plethysmogram can be worn to facilitate the monitoring of such symptoms. The log-linearized peripheral arterial viscoelastic index is expected to contribute to the improvement of QOL in various situations, such as monitoring of patients undergoing home medical care, support for early recovery, and daily healthcare.

Publications concerning this dissertation are listed in the bibliography [49–52].

Appendix A

Relationship Between Photoplethysmograms and Arterial Diameter Variations

Blood flow variations known as pulse waves caused by the beating of the heart propagate toward the peripheral artery, and can be measured. The two types are pressure pulse waves, which can be monitored to determine pressure fluctuations, and volume pulse waves, which can be monitored to determine arterial volume changes. Photoplethysmograms correspond to the latter type.

Using I_i to denote the intensity of LED-emitted incident light in relation to finger thickness D and I_o to denote the intensity of transmitted light, it follows from Lambert-Beer's law [53] that

$$A_D \equiv \log(I_i/I_o) = ECD. \tag{A.1}$$

Here, A_D is absorbance relating to finger thickness D, which is proportional to the density C of the relevant light-absorbing material, and E is an absorbance constant unique to the material in question [32, 33]. Changes in absorbance ΔA_D and in the

intensity of transmitted light ΔI_o are expressed as follows [32, 33]:

$$\begin{aligned} \Delta A_D &= A_D(r) - A_D \\ &= \log(I_o/I_o(r)) = EC(D(r) - D), \qquad \text{(A.2)} \\ \Delta I_o &= I_o - I_o(r). \qquad \text{(A.3)} \end{aligned}$$

Here, $r(t)$ is the diameter of the blood vessel at the arbitrary time t, and $D(r)$ is finger thickness. The photoplethysmogram $P_l(t)$ is a measure of ΔA_D. However, the change in absorbance ΔA_D can be generally approximated as follows with commercial equipment [32, 33]:

$$\begin{aligned} \Delta A_D &= \log(I_o/(I_o - \Delta I_o)) \\ &\simeq \Delta I_o/I_o. \qquad \text{(A.4)} \end{aligned}$$

It should be noted that $D(r) - D$ in Equation (A.2) is the arterial diameter $dr(t)$. EC in Equation (A.2) is defined as the proportional constant k_p, and the photoplethysmogram offset produced by the Equation (A.4) approximation is defined as P_{l0}. The photoplethysmogram $P_l(t)$ can be expressed as follows using Equation (A.2):

$$P_l(t) = k_p dr(t) + P_{l0}. \qquad \text{(A.5)}$$

Appendix B

A Log-linearized Gaussian Mixture Network

The log-linearized Gaussian mixture network (LLGMN) is a feed-forward neural network based on logarithm linearization of the Gaussian mixture model. The LLGMN learns data on statistical distribution based on the model included in the LLGMN, calculates a posterior probability for each configuration input, and identifies patterns in the learning data. To represent normalized distribution corresponding to each component of a Gaussian mixture model as weight coefficients of the LLGMN, the input vectors $\boldsymbol{x}$=$[x_1, x_2, \cdots, x_8]^{\mathrm{T}} \in \Re^8$ are first converted to form the modified input vector $\boldsymbol{X}$ as follows:

$$\boldsymbol{X} = [1, \boldsymbol{x}^{\mathrm{T}}, x_1^2, x_1x_2, \cdots, x_1x_8, x_2^2, x_2x_3, \cdots, x_2x_8, \cdots, x_8^2]^{\mathrm{T}}. \tag{B.1}$$

The first layer of the network consists of $H = 45$ units corresponding to the dimension of $\boldsymbol{X}$, and the identity function is used for the activation function of each unit. The relationship between the input and output of each unit in the first layer is defined as

$$^{(1)}I_h = X_h, \tag{B.2}$$

$$^{(1)}O_h = {}^{(1)}I_h. \tag{B.3}$$

Here, ${}^{(1)}I_h$ and ${}^{(1)}O_h$ denote the input and output, respectively, of the hth unit in the first layer.

When there are two classes and M_c components in class c, the second layer consists of $\sum_{c=1}^{C} M_c$ units. Each unit $\{c, m\}$ $(c = 1, 2, m = 1, \cdots, M_c)$ receives the output of the first layer weighted by the coefficient $w_h^{(c,m)}$. The input to the unit $\{c, m\}$ in the second layer ${}^{(2)}I_{c,m}$ and the output ${}^{(2)}O_{c,m}$ are defined as

$$ {}^{(2)}I_{c,m} = \sum_{h=1}^{H} {}^{(1)}O_h w_h^{(c,m)}, \tag{B.4} $$

$$ {}^{(2)}O_{c,m} = \frac{\exp[{}^{(2)}I_{c,m}]}{\sum_{c=1}^{2}\sum_{m=1}^{M_c}\exp[{}^{(2)}I_{c,m}]}. \tag{B.5} $$

Here, $w_h^{(c,m)}$, which is a parameter used in the Gaussian mixture model, is developed as weight coefficients of the LLGMN, and $w_h^{(2,M_2)} = 0$.

Finally, the third layer consists of two units corresponding to the number of classes, and the unit c integrates the outputs of M_c units $\{c, m\}$ $(c = 1, 2, m = 1, \cdots, M_c)$ in the second layer. The relationship between ${}^{(3)}I_c$ and output ${}^{(3)}O_c$ is defined as

$$ {}^{(3)}I_c = \sum_{m=1}^{M_c} {}^{(2)}O_{c,m}, \tag{B.6} $$

$$ {}^{(3)}O_c = {}^{(3)}I_c. \tag{B.7} $$

In the LLGMN defined above, the a posteriori probability $P(c|\boldsymbol{x})$ of each class c is defined as the output of the last layer ${}^{(3)}O_c$.

When the supervised learning of the LLGMN with the teacher vector $\boldsymbol{T}^{(n)} = [T_1^{(n)}, \cdots, T_c^{(n)}, \cdots, T_C^{(n)}]^T$ for the nth input vector $\boldsymbol{x}^{(n)}$ $(n = 1, \cdots, N)$ is given, the network energy function is determined as

$$ J = -\sum_{n=1}^{N} J_n = -\sum_{n=1}^{N}\sum_{c=1}^{2} T_c^{(n)} \log {}^{(3)}O_c^{(n)}. \tag{B.8} $$

and learning is performed to minimize it based on Kullback-Leibler information for true distribution. The weight modification $\Delta w_h^{(c,m)}$ of the corresponding weight $w_h^{(c,m)}$ is defined as

$$\Delta w_h^{(c,m)} = -\eta \sum_{c=1}^{C} \sum_{n=1}^{N} \frac{\partial J_n}{\partial w_h^{(c,m)}}. \tag{B.9}$$

Here, η is the learning rate, and the partial derivative in Equation (B.9) can be obtained using the chain rule in the same manner as the error backpropagation rule:

$$\begin{aligned} \frac{\partial J_n}{\partial w_h^{(c,m)}} &= \frac{\partial}{\partial w_h^{(c,m)}} (-\sum_{c=1}^{C} T_c^{(n)} \log^{(3)} O_c^{(n)}) \\ &= ({}^{(2)}O_c^{(n)} - \frac{{}^{(2)}O_c^{(n)}}{{}^{(3)}O_c^{(n)}} T_c^{(n)}) X_h^{(n)}, \end{aligned} \tag{B.10}$$

Here, the parameters of the Gaussian mixture model are learnt as weight coefficients of the LLGMN.

Bibliography

[1] M. Kuno, H. Ando, I. Sugihara, K. Akita, *Structure, Function and Materials of the Human Body IX, Nervous System (2)*, Tokyo, Japan: Japan Medical Journal, 93p, 2005.

[2] Primary hyperhidrosis (Fiscal year 2011), Japan Intractable Diseases Information Center, Japan, [Online], Available: `http://www.nanbyou.or.jp/entry/2430` (accessed on December 1st, 2015)

[3] T. Tanaka, H. Yokozeki, I. Katayama, M. Kaneda, N. Tamura, N. Sugano, H. Yshioka, Y. Tamada, S. Shinomiya: "Primary Localized Hyperhidrosis Practice Guideline", *The Japanese Journal of Dermatology*, vol. 120, no. 8, pp. 1607–1625, 2010.

[4] C. Drott, G. Göthberg, G. Claes, "Endoscopic Transthoracic Sympathectomy: An Efficient and Safe Method for the Treatment of Hyperhidrosis", *Journal of the American Academy of Dermatology*, vol. 33, no. 1, pp. 78–81, 1995.

[5] N. Yanagisawa, *Parkinson's Disease –Diagnosis and Treatment–*, Tokyo, Japan: Kanehara, 250p, 2000.

[6] M. M. Hoehn and M. D. Yahr, "Parkinsonism, Onset, Progression and Mortality", *Neurology*, vol. 17, no. 5, pp. 427–442, 1967.

[7] S. Fahn, R. L. Elton, and members of the UPDRS Development Committee, "Unified Parkinson's Disease Rating Scale. In: S. Fahn, C. D. Marsden, D. B. Calne, M. Goldstein, and editors, Recent Developments in Parkinson's Disease", *Macmillan Health Care Information*, vol. 2, pp. 153–163, 1987.

[8] K. Shima, E. Kan, T. Tsuji, A. Kandori, M. Yokoe, and Saburo Sakoda, "A Motor Function Evaluation System for Finger Tapping Movements Using Magnetic Sensors", *The Japanese journal of medical instrumentation*, vol. 78, no. 12, pp. 909–918, 2008.

[9] R. Okuno, K. Hamada, M. Yokoe, K. Abe, S. Sakoda, and K. Akazawa, "Development of a Finger-tapping Acceleration Measurement System for Quantitative Diagnosis of Parkinson's Disease", *Transactions of the Japanese Society for Medical and Biological Engineering*, vol. 43, no. 4, pp. 752–761, 2005.

[10] K. Morita, "History of Pain and Anesthesia", *Journal of the Japan Society of Acupuncture and Moxibustion*, vol. 58, no. 2, pp. 154–155, 2008.

[11] K. Toyota and S. Sakura, "Choice of Concentration, Volume and Dosage of Local Anesthetics in Epidural Anesthesia", *The Journal of Japan Society for Clinical Anesthesia*, vol. 28, no. 1, pp. 79–84, 2008.

[12] M. S. Avidan, L. Ahang, B. A. Burnsige, K. J. Finkel, A. C. Searleman, J. A. Selvidge, L. Saager, M. S. Turner, S. Rao, M. Bottros, C. Hantler, E. Jacobsohn, and A. S. Evers, "Anesthesia Awareness and the Bispectral Index", *The New England Journal of Medicine*, vol. 358, no. 11, pp. 1097–1108, 2008.

[13] E. Narimatsu, T. Niiya, A. Namiki, "Neuromuscular Disorders Affecting Neuromuscular Monitor Information", *The Journal of Japan Society for Clinical Anesthesia*, vol. 29, no. 1, pp. 23–34, 2009.

[14] B. T. Shahani, J. J. Halperin, P. Boulu, and J. Cohen, "Sympathetic Skin Response–a Method of Assessing Unmyelinated Axon Dysfunction in Peripheral Neuropathies", *Journal of Neurology, Neurosurgery, and Psychiatry*, vol. 47, no. 5, pp. 536–542, 1984.

[15] S. Akselrod, D. Gordon, A. Ubel, D. C. Shannon, A. C. Barger, and R. J. Cohen, "Power Spectrum Analysis of Heart Rate Fluctuation: a Quantitative Probe of Beat-to-beat Cardiovascular Control", *Science*, vol. 213, no. 4504, pp. 220–222, 1981.

[16] K. Shirahama, M. Tanaka, A. Matsuo, Z. Nagasawa, H. Ueda, "Evaluations of Heart Rate Variability (HRV) in the Patient Performed by Endoscopic Transthoracic Sympathectomy (ETS)", *Japanese Journal of Medical Technology*, vol. 48, no. 12, pp. 1673–1677, 1999.

[17] M. Kunimoto, "Taii Henkan test (Postural Change Test): Head–Up Tilt Test", *Autonomic Nervous Function Test. fourth edition*, Tokyo, Japan: Bunkodo, pp. 129–133, 2007.

[18] M. Moyoshi, K. Yokoyama, Y. Watanabe, K. Takata, S. Mukai, A. Okada, J. Hayano, "Analysis of Autonomous Nerve Response to Tilt Test by New HRV Parameters", *Japanese Journal of Medical Electronics and Biological Engineering*, vol. 34, no. 2, pp. 161–170, 1996.

[19] T. Fukushima, Y. Unezaki, H. Inoue, "Evaluation of the Effect of Dental Treatment on the Autonomic Nervous System using Power Spectral Analysis of Heart Rate Variability", *Journal of Osaka Odontological Society*, vol. 67, no. 2, pp. 195–200, 2004.

[20] A. Kagaya, Y. Nakamura, *Regulation of Blood Flow During Exercise –Present and Future–*, Tokyo, Japan: NAP, 310p, 2001.

[21] I. Korhonen and A. Yli-Hankala, "Photoplethysmography and Nociception", *Acta Anaesthesiologica Scandinavica*, vol. 53, no. 8, pp. 975–985, 2009.

[22] R. Nakamura, N. Saeki, A. Kutluk, K. Siba, T. Tsuji, H. Hamada, and M. Kawamoto, "Arterial Mechanical Impedance is a Sensitive Stress Response Monitor During General Anesthesia", *Hiroshima Journal of Medical Sciences*, vol. 58, no. 4, pp. 75–82, 2009.

[23] A. Sakane, T. Tsuji, Y. Tanaka, N. Saeki, and M. Kawamoto, "Monitoring of Vascular Conditions Using Plethysmogram", *Transactions of the Society of Instrument and Control Engineers*, vol. 40, no. 12, pp. 1236–1242, 2004.

[24] R. Busse, R. D. Bauer, A. Schabert, Y. Summa, P. Bumm, and E. Wetterer, "The Mechanical Properties of Exposed Human Common Carotid Arteries in vivo", *Basic Research in Cardiology*, vol. 74, no. 5, pp. 545–554, 1979.

[25] K. Hayashi, H. Handa, S. Nagasawa, A. Okumura, K. Moritake, "Stiffness and Elastic Behavior of Human Intracranial and Extracranial Arteries", *Journal of Biomechanics*, vol. 13, no. 2, pp. 175–184, 1980.

[26] S. Nagasawa, Y. Naruo, A. Okumura, K. Moritake, K. Hayashi, and H. Handa, "Mechanical Properties of Canine Femoral Artery Smooth Muscle", *The Journal of Japanese College of Angiology*, vol. 20, no. 4, pp. 221–226, 1980.

[27] A. Satoh, T. Serita, I. Tomita, H. Satoh, K. Iwanaga, H. Takashima, M. Tsujihata, "Loss of ^{123}I-MIBG Uptake by the Heart in Parkinson's Disease: Assessment of Cardiac Sympathetic Denervation and Diagnostic Value", *Journal of Nuclear Medicine*, vol.40, no. 3, pp. 371–375, 1999.

[28] A. Holdage, S. Asha, J. Craig, and J. Thompson, "Comparison of a Verbal Numeric Rating Scale with the Visual Analogue Scale for the Measurement of Acute Pain", *Emergency Medicine* (*Fremantle, W.A.*), vol. 15, no. 5–6, pp. 441–446, 2003.

[29] F. Berthier, G. Potel, P. Leconte, M. D. Touze, and D. Baron, "Comparative Study of Methods of Measuring Acute Pain Intensity in an ED", *The American Journal of Emergency Medicine*, vol. 16, no. 2, pp. 132–136, 1998.

[30] K. Ho, J. Spence, and M. F. Murphy, "Review of Pain-Measurement Tools", *Annals of Emergency Medicine*, vol. 27, no. 4, pp. 427–432, 1996.

[31] H. Shimazu, S. Seno, S. Kato, H.Kobayashi, M. Akimoto, "Development of a Quantitative Measurement Method for the Magnitude of Pain Using Painless Electrical Stimulation and Its Evaluation Using Experimental Pain", *Transactions of the Japanese Society for Medical and Biological Engineering*, vol. 43, no. 1, pp. 117–123, 2005.

[32] T. Ukawa, "Pulse Oximater", *Modern Medical Laboratory*, vol. 22, no. 1, pp. 11–16, 1994.

[33] T. Aoyagi and T. Ukawa, "Pulse Oximeter Which the Optical Measurement Produced. Structure and Principle of a Pulse Oximeter," *Clinical Engineering*, vol. 7, no. 2, pp. 102–110, 1996.

[34] T. Takemiya, J. Maeda, J. Suzuki, Y. Nishihira, M. Shimoda, "Differential Digital Photoplethysmographic Observations of Finger Vascular Exponential Response to the Arm Position Changes in Humans", *Advances in Exercise and Sports Physiology*, vol. 2, no. 2, pp. 83–90, 1996.

[35] K. Matsuda, *Seirigakutaikei III -Junkan no Seirigaku* (*Physiology System III - Physiology of Circulation-*), Tokyo, Japan: Igaku-Shoin, 1033p, 1969.

[36] C. C. Lin, L. R. Mo, L. S. Lee, S. M. Ng, M. H. Hwang, "Thoracoscopic T2-sympathetic Block by Clipping – A Better and Reversible Operation for Treatment of Hyperhidrosis Palmaris: Experience with 326 Cases", *The European Journal of Surgery. Supplement*, vol. 164, pp. 13–16, 1998.

[37] N. Yoshimura, T. Kumazawa, O. Yuge, and H. Furuya, *Hyojun Masuikagaku* (*STANDARD TEXTBOOK*). *fourth edition*, Tokyo, Japan: Igaku-Shoin, 558p, 2002.

[38] R. Ochi, *Seirigaku Text* (*Physiology Text*) *fourth edition*, Tokyo, Japan: Bunkodo, 525p, 2003.

[39] W. M. Bayliss, "On the Local Reactions of the Arterial Wall to Changes of Internal Pressure", *The Journal of Physiology*, vol. 28, no. 3, pp. 220–231, 1902.

[40] Department of Anesthesiology, Yokohama City University, School of Medicine, *Anesthesia Handbook. second edition* Tokyo, Japan: Chugai-Igakusha, 361p, 2001.

[41] G. L. Willis and E. J. D. Turner, "Primary and Secondary Features of Parkinson's Disease Improve with Strategic Exposure to Bright Light: A Case Series Study", *Chronobiology International*, vol. 24, no. 3, pp. 521–537, 2007.

[42] T. Tsuji, O. Fukuda, H. Ichinobe, and M. Kaneko, "A Log-Linearized Gaussian Mixture network and Its Application to EEG Pattern Classification", *IEEE Transactions on Systems, Man, and Cybernetics, Part C: Applications and Reviews*, vol. 29, no. 1, pp. 60–72, 1999.

[43] M. Konagaya, "Multiple System Atrophy", *Japanese Journal of National Medical Services*, vol. 57, no. 3, pp. 159–165, 2003.

[44] A. Kohno, A. Kutluk, T. Tsuji, T. Ukawa, R. Nakamura, N. Saeki, M. Yoshizumi, M. Kawamoto, "Quantitative Evaluation of Pain with Mechanical Nociceptive Stimuli by the Change of Arterial Wall Viscoelasticity", *The Japanese Journal of Medical Instrumentation*, vol. 80, no. 3, pp. 196–204, 2010.

[45] J. D. Loeser and R. Melzack, "Pain: An Overview", *Lancet*, vol. 353, no. 9164, pp. 1607–1609, 1999.

[46] T. Koganezawa and N. Terui, "Autonomic Reflex: Cardiovascular System", *Autonomic Nervous Function Test. fourth edition*, Tokyo, Japan: Bunkodo, pp. 43–49, 2007.

[47] H. Saito, "Autonomic Reflex: Sweating & Dermovascular System", *Autonomic Nervous Function Test. fourth edition*, Tokyo, Japan: Bunkodo, pp. 50–57, 2007.

[48] K.Aihara, T.Takebe, and M.Toyoda, "Chaotic Neural Networks", *Physics Letters A*, vol. 144, no. 6–7, pp. 330–340, 1990.

[49] H. Hirano, T. Horiuchi, H. Hirano, Y. Kurita, T. Ukawa, R. Nakamura, N. Saeki, M. Yoshizumi, M. Kawamoto, and T. Tsuji, "A Log-linearized Peripheral Arterial Viscoelastic Index and Its Application to Endoscopic Thoracic Sympathectomy," *Transactions of the Society of Instrument and Control Engineers*, vol. 48, no. 11, pp. 731–739, 2012.

[50] H. Hirano, T. Horiuchi, H. Hirano, Y. Kurita, T. Ukawa, R. Nakamura, N. Saeki, M. Yoshizumi, M. Kawamoto, and T. Tsuji, "Monitoring of Peripheral Vascular Condition Using a Log-Linearized Arterial Viscoelastic index During Endoscopic Thoracic Sympathectomy," *35th Annual International Conferenc of the IEEE Engineering in Medicin and Biology Society*, pp.2587–2590, Osaka, Japan, July, 2013.

[51] H. Hirano, M. Ito, T. Endo, H. Hayashi, H. Hirano, Y. Kurita, S. Sakoda, T. Tsuji, "A diagnostic support method for evaluating autonomic nervous function of patients with Parkinson's disease using a head-up tilt test," *The Japanese journal of medical instrumentation*, vol. 85, no. 6, pp. 569–576, 2015.

[52] H. Matsubara, H. Hirano, H. Hirano, G. Matsuoka, Y. Kurita, T. Ukawa, R. Nakamura, N. Saeki, M. Yoshizumi, M. Kawamoto, and T. Tsuji, "Quantification of Sympathetic Nervous Activity Based on Log-linearized Peripheral Arterial Viscoelastic Model and Its Application to Objective Assessment of Pain during Electrocutaneous Stimulation," *Transactions of the Society of Instrument and Control Engineers*, vol. 51, no. 9, pp. 627–633, 2015.

[53] R. A. Day and A. L. Underwood, *Quantitative Analysis. fourth edition*, New Jersey, the United States: Prentice-Hall, 660p, 1980.

Acknowledgments

I wish to thank my advisor, Professor Toshio Tsuji, Biological Systems Engineering Laboratory, Division of Electrical, Systems and Mathematical Engineering, Institutre of Engineering, Hiroshima University for his advice, suggestions, encouragement, and patience. He has taught me in the various research fields of neural networks, welfare applications, robotics and medical applications. His serious attitude toward research has been an excellent example to me.

I would like to acknowledge committee members Professor Idaku Ishii and Professor Toru Yamamoto, Division of Electrical, Systems and Mathematical Engineering, Institutre of Engineering, Hiroshima University, for their invaluable suggestions and discussions on this dissertation. I am deeply grateful to Professor Masashi Kawamoto, Assistant Professor Noboru Saeki, Assistant Professor Ryuji Nakamura, Department of Anesthesiology and Critical Care, Division of Clinical Medical Science, Institute of Biomedical & Health Sciences, Hiroshima University, Professor Masao Yoshizumi, Department of Cardiovascular Physiology and Medicine, Division of Molecular Medical Science, Institute of Biomedical & Health Sciences, Hiroshima University, Dr. Teiji Ukawa, Nihon Kohden Corporation, Dr. Saburo Sakoda, the director of Toneyama National Hospital, Dr. Takuyuki Endo, a medical doctor of Toneyama National Hospital, Mr. Kouji Fujisaki, a clinical laboratory technologist of Toneyama National Hospital, Associate Professor Yuichi Kurita, Biological Systems Engineering Laboratory, Divi-

sion of Electrical, Systems and Mathematical Engineering, Institutre of Engineering, Hiroshima University, and Assistant Professor Harutoyo Hirano, College of Engineering, Academic Institute, Shizuoka University, for their advice, suggestions and kind support in the medical field.

I must also take this opportunity to acknowledge Mr. Hiromi Maruyama, Mr. Tetsuya Horiuchi, Mr. Hideaki Hayashi, Mr. Masafumi Ito, Mr. Hiroki Matsubara, Ms. Nami Kiyoto, the other members of Medical Engineering group and all the other members in the Biological Systems Engineering Laboratory, Department of System Cybernetics, Graduate School of Engineering, Hiroshima University for their encouragement and support.

Last but not least, my deepest gratitude goes to my family for their encouragement and support in my life.

My Ph.D. study was supported in part by a Grant-in-Aid for Scientific Research (26·6779) from the Research Fellowships for Young Scientists of the Japan Society for the Promotion of Science.